This article has been accepted for publication in Environmental Science and Technology (Published by ASC) and should be cited as:

Nawras Ghanem, Claire E. Stanley, Hauke Harms, Antonis Chatzinotas, Lukas Y. Wick. 2019. Mycelial effects on phage retention during transport in a microfluidic platform. *Envrionmental Science and Technology*, **53**: 11755-11763.

First Published: 18 September 2019 https://doi.org/10.1021/acs.est.9b03502

MYCELIAL EFFECTS ON PHAGE RETENTION DURING TRANSPORT IN A MICROFLUIDIC PLATFORM

Nawras Ghanem[1], Claire E. Stanley[2], Hauke Harms[1,3], Antonis Chatzinotas[1,3] and Lukas Y. Wick[1]*

[1]Helmholtz Centre for Environmental Research - UFZ, Department of Environmental Microbiology, Permoserstraße 15, 04318 Leipzig, Germany.

[2]Agroecology and Environment Research Division, Agroscope, Reckenholzstrasse 191, 8046 Zurich, Switzerland

[3]German Centre for Integrative Biodiversity Research (iDiv) Halle-Jena-Leipzig, Deutscher Platz 5e, 04103 Leipzig, Germany

Running title: Transport of tracer phages along mycelia

Intended for: Environmental Science and Technology

* Corresponding author: Helmholtz Centre for Environmental Research - UFZ. Department of Environmental Microbiology; Permoserstrasse 15; 04318 Leipzig, Germany. Phone: +49 341 235 1316, fax: +49 341 235 45 1316, e-mail: lukas.wick@ufz.de.

ABSTRACT

Phages (i.e. viruses that infect bacteria) have been considered as good tracers for the hydrological transport of colloids and (pathogenic) viruses. Little, however, is known about interactions of phages with (fungal) mycelia as the prevalent soil microbial biomass. Forming extensive and dense networks, mycelia provide significant surfaces for phage-hyphal interactions. Here, we for the first time quantified the mycelial retention of phages in a microfluidic platform that allowed for defined fluid exchange around hyphae. Two common lytic tracer phages (*Escherichia coli* phage T4 and marine phage PSA-HS2) and two mycelia of differing surface properties (*Coprionopsis cinerea*, *Pythium ultimum*) were employed. Phage-hyphal interaction energies were approximated by the extended Derjaguin-Landau-Verwey-Overbeek (XDLVO) approach of colloidal interaction. Our data show initial hyphal retention of phages of up to $\approx 4 \times 10^7$ PFU mm^{-2} ($\approx$ 2550 PFU mm^{-2} s^{-1}) with a retention efficiency depending on the hyphal and, to a lesser extent, the phage surface properties. Experimental data were supported by XDLVO calculations, which revealed the highest attractive forces for the interaction between hydrophobic T4 phages and hydrophobic *C. cinerea* surfaces. Our data suggest that mycelia may be relevant for the retention of phages in the subsurface and need to be considered in subsurface phage tracer studies. Mycelia-phage interactions may further be exploited for the development of novel strategies to reduce or hinder the transport of undesirable (bio-)colloidal entities in environmental filter-systems.

KEYWORDS: marine phages, tracer, hyphae, microfluidic platform, transport, mycelia

TOC / ABSTRACT ART

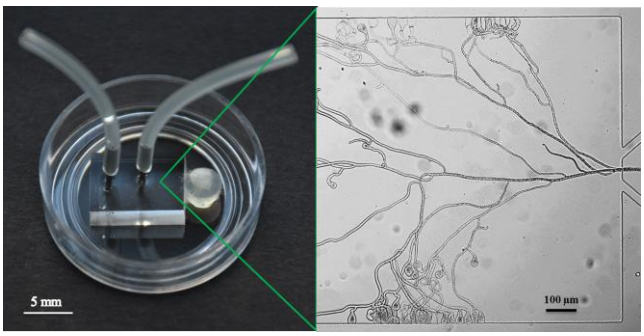

INTRODUCTION

Previous work has highlighted the relevance of phages (i.e. viruses that infect bacteria)[1,2] as promising tracers for fecal contamination or for the evaluation of colloidal and water transport.[3,4,5] Although phage tracers have significantly improved our understanding of water and colloid movement in aquifers[6], information on the transport of phage tracers in the complex soil subsurface is still limited, yet highly needed. For example, accurate descriptions of microbial (colloid) transport and soil-related transport drivers are needed to assess the risk of pathogen contamination to drinking water supplies or to develop control strategies and treatment options. Although still rarely applied, marine tracer phages hold much promise as tracers in subsurface ecosystems, as they and their hosts are absent in terrestrial ecosystems. Typically, up to 10^{15} phages (~1 g) can be applied and phage concentrations of < 10 phages mL^{-1} of recovered water can be detected[7] by specific interactions with their host bacteria using plaque forming unit (PFU) assays.[7,8,9,10] Subsurface transport of phages (and other viruses) is driven by environmental factors, phage type and phage interaction with autochthonous soil microorganisms.[11] Environmental factors included soil type and texture,[12,13,14,15] electrolyte composition[16,17] or the degree of water saturation in soil.[11,18,19] Other research assessed the influence of virus characteristics such as the effect of the isoelectric point,[20] combinations of size and isoelectric point[21] or the morphology of phages and other viruses.[22] While abiotic environmental drivers have been widely studied, insufficient knowledge exists concerning interactions of phages and viruses with non-host microbes (termed in the following as unspecific phage-microbe interactions). Such interactions may be of high importance for the transport and survival of pathogens in soil and the upper layer of the Earth's Critical Zone (CZ)[23], i.e. the thin, living and permeable layer that connects the atmosphere with the geosphere. Research on unspecific phage-microbe interactions mainly evaluated the influence of sterile vs. non-sterile conditions on the fate of phages.[24] These studies suggest better survival of phages and other viruses in sterile rather than in non-sterile environments.[24,25,26] Other studies have highlighted the role of fungi as mediators for the virulence of plant viruses.[27,28,29] To our knowledge, however, no literature exists

on unspecific interactions of phages with hyphal surfaces or the effect of (fungal) mycelia on waterborne transport of phages.

Fungi occur in nearly every aerobic habitat, being important drivers of biogeochemical cycles[30,31] and fertility of soils. Being the major microbial biomass in soil, they typically develop a spatially extensive mycelium, which comprises up to 1000 m of hyphae per gram of dried soil.[32,33] Mycelia also provide ideal 'logistic networks' for bacterial evolution[34,35,36] as well as the transport of bacteria. Fungal growth is not restricted to saturated environments, as their hyphae are also able to breach air-water interfaces[37] and thereby connect different soil microenvironments.[32] Of central importance for possible phage transport is the observation that hyphae may change the physico-chemical properties of their surface[38] and hence, alter the water infiltration properties of soils through the production of large amounts of hydrophobic compounds in the outer cell wall.[39]

Here, we hypothesized that mycelia might retain phages, due to the physico-chemical interactions of phages with hyphal surfaces, and hence would influence waterborne phage transport. Using a well-controlled microfluidic platform, we quantified the effects of mycelia on phage retention and transport at the micrometer scale. The microfluidic platform allowed single hyphae to be subjected to a defined concentration of phages and to quantify their interactions by comparing the in- and outflow concentrations of phages. Two lytic phages commonly used as tracers to follow pathogen contamination (*E. coli* T4 phage) or colloidal particle transport[22] (marine phage PSA-HS2) were used as models. The phages belong to different virus families[40,41] and vary in their morphology and physico-chemical surface properties. Two filamentous soil organisms (*Coprinopsis cinerea* and *Pythium ultimum*) of varying surface hydrophobicity were also implemented. Experimental observations were accompanied by the extended Derjaguin-Landau-Verwey-Overbeek approach (XDLVO) of colloidal interaction that describes the forces between charged surfaces interacting in a liquid medium. Our findings suggest that the mycosphere may significantly influence the transport and fate of phages and phage tracers.

MATERIALS AND METHODS

Organisms and culture conditions

Two well-characterized lytic tracer phages were studied (Table 1). The T4 coliphage (T4)[42] and its host *E. coli* (Migula 1895)[43] were purchased from Deutsche Sammlung von Mikroorganismen und Zellkulturen GmbH (DSMZ, Germany), while the marine phage PSA-HS2 and its host strain *Pseudoalteromonas* H13-15 were kindly provided by Dr. B. M. Duhaime (University of Michigan, USA).[44] The T4 coliphage (*Myoviridae*) and the PSA-HS2 (*Siphoviridae*) are of different morphology. Both phages were propagated, purified and counted as described previously.[22] *P.* H13-15 and *E. coli* were grown at room temperature using dilute (50%) 2216E medium[45] and Luria-Bertani (LB) medium[46]. Both phages were stored in SM buffer (100 mM NaCl, 8 mM $MgSO_4$ $7H_2O$, 50 mM Tris-HCl. pH 7). Phages were quantified by a modified spotting plaque assay technique[22] by incubating phage host pairs overnight either at room temperature (RT, 25ºC) (PSA-HS2) or at 37°C (T4 coliphage). The agaricomycete *C. cinerea* strain AmutBmut pMA412 (*C. cinerea*) and the oomycete *P. ultimum*[32] exhibit hyphal surfaces of varying hydrophobicity.[38] *C. cinerea* strain AmutBmut pMA412 constitutively expresses the red fluorescent protein dTomato.[47] *C. cinerea* and *P. ultimum* were cultivated on yeast-malt extract-glucose medium solidified with agar (YMG, Table S2) and Luria Bertani (LB) agar for three days at 30 °C and RT, respectively.[47,48]

Stability and viability of phage suspensions

Conditioned (i.e., cell-free) media were prepared by cultivating *C. cinerea* and *P. ultimum* in glucose-based liquid CCMM minimal[47] (Table S2) and LB media using a shaker incubator (SM-30, Edmund Bühler GmbH, Bodelshausen, Germany) at 150 rpm, at 30 °C for 9 d. Conditioned media were obtained by vacuum filtration of the mycelial suspensions using a glass frit (Schott pore 40, DURAN® filter funnel, DWK Life Sciences, Wertheim, Germany) and subsequently stored at 4 °C. The stability (i.e. phage aggregation and infectivity) of phage suspensions was investigated in batch experiments at

RT in 10 mL glass vials[49] containing 6 mL of phage suspensions (10^8-10^9 PFU mL^{-1}) in conditioned media (Fig. S1). Experiments were performed in triplicate by exposing phages to the conditioned media for 0, 4 and 22 h and subsequently performing a PFU quantification (Fig. S1). The stability of the phage suspensions was calculated as the ratios of phage concentrations (Table 2). Similar experiments were performed using fresh media as controls (Fig. S2).

Characterization of physico-chemical surface properties

The contact angles of water θ_w, formamide θ_f, and methylene iodide θ_{mi} were measured using a DSA 100 drop-shape analysis system (Krüss GmbH, Hamburg, Germany). Briefly, mycelia of the organisms were cultivated for 2 - 3 days on a 0.45 µm-filter (NC 45, Cellulose Nitrate Membrane Whatman, Maidstone, Kent, United Kingdom) placed on the surface of LB (*P. ultimum*) or YMG agar plate (*C. cinerea*). Filters covered with fungi were removed and mounted on a microscope slide and the contact angles measured as detailed elsewhere.[38,50] The zeta-potential (ζ) for the mycelia of *C. cinerea* and *P. ultimum* were approximated from the electrophoretic mobility of hyphal elements measured by Doppler electrophoretic light scattering analysis (Zetamaster, Malvern Instruments, Malvern, UK). Mycelia of both organisms were cultivated for 3 days as described above. The biomass was then carefully scratched off the filter using a sterile spatula, suspended in 1 mL of SM buffer (100 mM, pH = 7) and homogenized using a micro-blender according to Potter-Elvehjem (Carl Roth GmbH + Co, Germany) prior to zeta potential measurement. The zeta potential of PSA-HS2 and T4 phage suspensions (SM buffer; 100 mM, pH = 7) was approximated as described earlier.[22]

Phage transport experiments

Microfluidic device design and preparation

Microfluidic devices were prepared as described in Stanley et al.[47] based on a channel architecture[51] that enables laminar flow conditions as a result of actively pumping solutions into the observation chamber (Figs. 1 & S3; cf. SI for detailed description).

Incubation and visualization of mycelial growth structures

Using a syringe (Injekt®Solo, 2 mL, B. Braun, Melsungen, Germany), the microfluidic devices were filled with either liquid LB medium for *P. ultimum* or glucose-based CCMM for *C. cinerea*. A small agar plug (≈ 6 mm^2) containing the fungal inoculum was placed next to the opening of the microfluidic channel (Fig. 1). The microfluidic devices were incubated for 24 h (*P. ultimum*) and 48 h (*C. cinerea*) in a humid and dark environment to allow the mycelia to reach the end of the observation channel. Prior to the addition of the phages, the mycelial structure in the observation channel was determined using an AZ100M fluorescence microscope (Nikon, Düsseldorf, Germany) and Nikon NIS-Elements software. The surface area of the mycelia in the observation chamber ($A_{mycelia}$) was approximated based on the total length of the mycelia in the observation chamber assuming hyphae to be tubes having a diameter of 7 ± 1 µm (*C. cinerea*)[47] and 10 ± 3 µm (*P. ultimum*) using ImageJ software[52] following a modified method described by Jenson et al. (Table 1). [53]

Quantification of phage Mass recovery

The mass recovery (M) was calculated as the ratio of the total number of phages in the effluent and the influent in a given time period (Δt) as inferred from the difference of inlet (C_o) and outlet (C_t) phage concentration as described by eq. 1

$$M = \frac{\sum C_t \Delta t}{\sum C_0 \Delta t} * 100 \qquad (1)$$

Quantification of phage retention

Prior to addition of phage suspensions the microfluidic devices were carefully flushed with ≈ 100 µL of SM buffer (100 mM, Ionic strength I_s ~ 360 mM) to replace the growth media. A syringe pump (KD

Scientific Inc., USA) loaded with Luer-lock syringes (Injekt®Solo, 2 mL, B. Braun, Melsungen, Germany) was used to administer the phage suspension (≈ 3×10^9 PFU mL^{-1}) into the microfluidic channels at a volumetric flow rate of 5 µL h^{-1} (average velocity: 1.4×10^{-4} m s^{-1}; time for fluid to reach outflow: 43 s (cf. SI)).. After 4 and 22 h at RT, samples from the inlet and the outlet (i.e. aliquots from the well-mixed effluents after 0-4h (20 µL) and 4-22 h (90 µL)) of triplicate microfluidic devices containing mycelia were collected and the phages enumerated. Quadruplicate experiments in mycelia-free microfluidic devices (control) revealed insignificant (< 2 %) losses of phages in the devices and the tubing material (Fig. 2 & Table 2). The retention of phages to the mycelial surface (R_P) was calculated using eq. 2, with $C_{t,effluent}$ and $C_{t,influent}$ being the effluent and the influent phage concentrations respectively, $C_{t,\ effluent,\ control}$ the effluent phage concentrations in mycelia-free controls, $V_{t,effluent}$ the volume of effluent at sampling (20 µL and 90 µL after 4 h and 22 h, resp.) and $A_{mycelia}$ the estimated surface area of the mycelia in mm^2.

$$R_P = \frac{((C_{t,influent} - C_{t,effluent}) - (C_{t,influent} - C_{t,effluent,control})) * V_{t,effluent}}{A_{mycelia}} \quad (2)$$

The t-test (two-tailed distribution) was used to test for significance and to determine the level of marginal significance (p-value).

Calculations of phage-hyphal surface interaction energies

The total interaction energy (G_{XDLVO}) between phages and hyphal surfaces was predicted by the extended Derjaguin-Landau-Verwey-Overbeek (XDLVO) theory of colloidal interactions.[54] G_{XDLVO} is the sum of the electrostatic repulsion (G_{EDL}), the Lifshitz-van der Waals (G_{LW}) and the acid-base (G_{AB}) interaction energy. While G_{AB} compares the energy status between attached and nonattached situations, G_{EDL} and G_{LW} are functions of the separation distance, h (nm), between two surfaces[55,56] (eq. 3):

$$G_{XDLVO}(h) = G_{AB} + G_{EDL}(h) + G_{LW}(h) \quad (3)$$

Sphere-plate geometry was applied as phages are far smaller than the hyphal surfaces.[57] G_{EDL}, G_{LW} and G_{AB} were calculated as described previously.[22] Surface free energy calculations were based on measured contact angles of phages and fungi using water, formamide and methylene iodide as liquids (as described above) and the Young equation.[58] The Gibbs free energies (Table S1) and Hamaker constants were calculated using the surface free energies of studied phages and hyphal surfaces applying eq. S4 and eq. S11.

RESULTS

Phage transport in microfluidic devices

Interactions of phages with hyphal surfaces were investigated using a microfluidic platform under continuous flow conditions typical for subsurface water flows (1.2 m d^{-1}) [59] (Fig. 1) by comparing the in- and effluent phage concentrations (Fig. 2; Table 2). Control experiments in the absence of mycelia (Table 2, Fig S2) revealed negligible (<2 %) differences between in- and effluent phage concentrations (Table 2). Water contact angle measurements revealed that *C. cinerea* (θ_w = 131 ± 2°) and *P. ultimum* (θ_w = 62 ± 6°) were highly and moderately hydrophobic respectively. The T4 and PSA-HS2 phages were of similar size (≈ 200 nm) and surface charge ($\zeta \approx$ -10 mV) yet differed in surface hydrophobicity (T4: θ_w = 95°; PSA-HS2: θ_w = 40°; Table 1).

In the presence of *P. ultimum*, differences between the PFU counts of PSA-HS2 and T4 phages in the in- and effluents of the microfluidic devices were small (i.e., < 4 %) and statistically not significant ($p > 0.05$) at both time intervals (0 - 4 h and 4 - 22 h) (Fig. 2A & C and Table 2). The presence of highly hydrophobic *C. cinerea* hyphae, however, resulted in ≈ 25 % (PSA-HS2) and 90% (T4) reductions of the outflow concentration of the hydrophilic PSA-HS2 (Fig. 2B) and hydrophobic T4 phages (Fig. 2D) after 4h ($p \leq 0.05$). This corresponds to a mass recovery of M = 7 % (T4) and M = 77 % (PSA-HS2) during the first 4 h of phage percolation (Table 2). Most likely due to blocking effects of the hyphal collector (i.e., hyphal surface became progressively occluded), the retention of T4 phages was

minimized as similar PFU counts for the effluents and controls were observed after 22 h. As the hyphal density and morphology of the two mycelia differed (cf. Fig. 1C & D), micrographs of the hyphal structures in the observation chambers were taken, and the hyphal surface areas exposed to the percolating phages were estimated (Table 1). After 4 h, the calculated apparent (yet statistically not significant) retention of phages to the mycelial surface (R_P) of *P. ultimum* was ≈ 2.3×10^6 PFU mm^{-2} for T4 and 4.3×10^6 PFU mm^{-2} for phage PSA-HS2 (Table 2). The presence of the hydrophobic surface of *C. cinerea*, however, significantly retained both phages with $R_P = 13.6 \times 10^6$ PFU mm^{-2} for PSA-HS2 and $R_P = 36.7 \times 10^6$ PFU mm^{-2} for T4 phages ($p \leq 0.05$; Fig. 3). This results in estimated time-averaged deposition rates of 941 and 2550 PFU mm^{-2} s^{-1} for PSA-HS2 and T4, respectively (Table 2). Better phage retention by more hydrophobic mycelia of *C. cinerea* was also evidenced by smaller mass recovery of T4 and PSA-HS2 phages (Table 2).

Effect of mycelial conditioned media on phage infectivity and colloidal stability

As mycelial products may influence the stability and infectivity of phages, the effect of *P. ultimum* and *C. cinerea* conditioned media on the PFU counts of T4 and PSA-HS2 was quantified after exposing the phages to the conditioned media for 0, 4, and 22 h. After 4 h no statistically significant reduction on PSA-HS2 and T4 phage concentrations was observed (Table 2, Fig. S1). Similarly, no effects of the conditioned media on PSA-HS2 phage counts were observed after 22 h of exposure. By contrast, the highly hydrophobic T4 phages exhibited a slight, yet statistically significant ($p \leq 0.05$) decrease of ≈ 14 % PFU counts in the conditioned medium of *C. cinerea* yet not of *P. ultimum* (≈ 6 % decrease).

Approximation of phage-hyphal surface interaction energies

Phage-hyphal surface interaction energy (G_{XDLVO}) profiles were calculated using the XDLVO theory (cf. eq. 3 & eq. S2) based on the sphere-plate model (Fig. 4, Table 1).[57] This model is well-accepted approach to estimate the interaction energies of a phage approaching a surface,[57,60] although phages

are away from the uniform surfaces of colloidal particles. The G_{XDLVO} is characterized by three different interaction energies: the primary minimum (Φ_{min1}) as the deep energy at short separation distance *h* from the sorbent surface, the secondary minimum (Φ_{min2}) as the shallow energy at larger distances allowing for reversible phage adhesion, and the maximum energy barrier (i.e. the energy the phages need to overcome to get irreversibly attached at the Φ_{min1}) (Φ_{max1}).[61,62] For the given experimental conditions, the G_{XDLVO} profiles predicted either no (Φ_{max1}: no to be calculated) or low ($\Phi_{max1} = 4.7 \times 10^{-3}$ k_BT at $h \approx 10$ nm; PSA-HS2) maximum energy barriers for the interactions of *P. ultimum* with T4 and PSA-HS2 phages, respectively (Table 2, Fig. 4). This indicates that both phages, if retained by the hyphae of *P. ultimum*, would be attracted directly to the primary minimum Φ_{min1}. However, no T4 phage) and a very weak secondary minimum ($\Phi_{min2} = -2.7 \times 10^{-4}$ k_BT at $h \approx 12$ nm) for PSA-HS2 phage was calculated and, hence, poor reversible retention of both phages by *P. ultimum* surfaces predicted by the XDLVO approach.[63,64] For interactions of the hyphal surface of *C. cinerea*, the XDLVO approach predicted the absence of Φ_{max1} for both phages and more negative primary minima than for *P. ultimum* (Table 2, Fig. 4). No secondary minima were found, yet attractive G_{XDLVO} values, however, were calculated up to $h \approx 100$ nm and $h \approx 40$ nm above the *C. cinerea* hyphal surfaces for T4 and PSA-HS2 phages, respectively.

DISCUSSION

Effect of mycelia on phage transport and retention

We studied the interactions between phages and mycelia at the micrometer scale using a bespoke microfluidic platform. The so-called "Soil-on-a-Chip" microfluidic technology for organismal studies is an emerging field,[65] which allows for the precise control of the physico-chemical microenvironment, high-resolution imaging and the simulation of environmental complexity on the microscale.[66] We assessed the interaction of phages with hyphae both in a quantitative manner and at the level of single hyphae. To our knowledge, this is the first study of its kind to analyze the role of hyphae on the

transport and retention of nano-sized particles (phages). For this purpose, two lytic phages of different morphology and physical-chemical properties were applied, i.e., the T4 coli-phage and the marine phage PSA-HS2. The phages were injected into microfluidic channels containing growing mycelia of known structure and differing hydrophobicity and the time-averaged retention of the phages was calculated. Mycelia of the oomycete *P. ultimum* and of the hydrophobic agaricomycete *C. cinerea* were employed. Phage decay due to experimental conditions in the absence of mycelia was negligible and accounted for in our experiments. . Our data suggest that passage through microfluidic devices in the presence of moderately hydrophobic mycelia (*P. ultimum*) didn't lead to statistically verifiable phage retention (Table 2). The highly hydrophobic mycelia of *C. cinerea*, however, efficiently retained both phages (as reflected by increased R_P values) and significantly ($p \leq 0.05$) reduced mass recovery (T4: > 93 %; PSA-HS2: and > 23 %) relative to mycelia free controls (Table 2). Differences in the phage recovery also demonstrate higher retention of the hydrophobic phage T4 than of the more hydrophilic PSA-HS2 phage. Most likely due to saturation of possible sorption sites, T4 however, showed no significant additional retention by *C. cinerea* in the observation period up to 22 h (Fig. 2D) while apparent saturation of the hyphal surface for PSA-HS2 phages was not yet reached (Fig. 2C). Our findings are consistent with previous studies showing that hydrophobic phages (and other viruses) are more efficiently retained than hydrophilic phages[67,68,22] They further reveal that sorption of viruses strongly depends on the surface properties of both the viruses and the sorbent; for instance, positively charged sorbents have been considered as ideal materials for the removal of viruses from aqueous systems.[69,70] Our results likewise emphasize for the first time the role of hydrophobic interactions for the interaction between phages and hyphal surfaces.[67]

As hyphal metabolites or extracellular products are known to foster coagulation[71,39] and hence may reduce colloidal stability and possible infectivity of phages, we further studied the impact of mycelial conditioned media on the infectivity of T4 and PSA-HS2 phage suspensions. With the exception of a slight (14 %) reduction of T4 phage counts after 22 h, no influence of mycelial conditioned media on

total phage counts (i.e., phage infectivity) was observed (Fig. S1). Similar to the known effect of solid matrices,[72,73] it even may be speculated that fungal surfaces may protect viruses from inactivation.[72,73] The reasons for the reduction of T4 phages in the presence of *C. cinerea* conditioned medium after 22 h remain though unclear, yet are likely to be explained by the effect of extracellular mycelial products in the conditioned media (e.g., glycoprotein mucilages) that may influence colloidal stability rather than the infectivity of T4 phages. An additional effect on the reduced T4 phage stability may be caused by the CCMM medium, as mycelia-free controls also exhibited stability of 93 ± 4 % (Fig. S2). Our data hence suggest the absence of mycelial effects on the infectivity and colloidal stability of the phages in the microfluidic devices. They underpin the relevance of phage deposition as the main driver for the reduced mass recoveries observed in the presence of the hydrophobic surfaces of *C. cinerea*.

Phage-hyphal surface interaction energies

Phages are charged colloidal particles[69] and believed to follow the principles of colloid chemistry despite of their morphological and structural variability.[54] Applying the XDLVO approach, we calculated the surface interaction energies as a function of the surface-to-surface distance, *h*, for a phage approaching a mycelial surface (eq. 3, Fig. 4). The XDLVO interaction energy is characterized by the primary minimum (Φ_{min1}), the secondary minimum (Φ_{min2}) and the maximum energy barrier (Φ_{max1}).[57] The XDLVO calculations predicted poor interactions of T4 and PSA-HS2 phages with hyphal surfaces of *P. ultimum* as evidenced by shallow Φ_{min2} (-3×10^{-4} k_BT) for the PSA-HS2 phage[64] and poorly negative G_{XDLVO} profiles ($> \approx -8 \times 10^{-4}$ k_BT) at distances h > 10 nm above the surfaces for the T4 phage (Fig 4). Only at close distances (h < ≈10 nm) to the hyphal surface, phages with a small kinetic energy[57] would be able to overcome the very low maximum energy barriers and get (irreversibly) attached in the primary minimum. These predictions are in good agreement with our experimental results showing less phage retention by *P. ultimum* than by *C. cinerea* hyphal surfaces (Figs. 2 & 3). For the latter, the G_{XDLVO} profiles of T4 and PSA-HS2 interactions exhibited clearly

negative G_{XDLVO} values up to $h \approx 40$ nm (PSA-HS2: -1.73 k_BT at $h = 10$ nm to -0.06 k_BT at $h = 40$ nm) and up to $h \approx 145$ nm (T4: -3.62 k_BT at $h = 10$ nm to -0.06 k_BT at $h = 145$ nm) respectively and thus remain attractive up to longer separation distances than for hyphal surfaces of *P. ultimum* (Fig. 4). the XDLVO predictions reflect the experimentally observed differences of retention of T4 and PSA-HS2 phages by mycelia of *C. cinerea* and *P. ultimum* respectively (Fig. 2 & 3) and supports the applicability of XDLVO approach to study the interactions of phages with surfaces.[60]

Implications for phage transport

The mobilization of colloids or bio-colloids such as bacteria and viruses in soil often is triggered by, snowmelts, or thunderstorms or high-intensity rain events that lead to high loads of the seepage water.[74] Rapid waterborne transport thereby may occur along macro-pores, cracks, or faults of the partly saturated soil, and hence in cavities where mycelia and their thread-like, adaptive and fractal networks[75,76,35,36] may be typically found.[77] Depending on the soil type, filamentous fungi may exhibit dry weight biomasses of up to 45 t per ha[33] and corresponding hyphal lengths of up to 10^2 m g^{-1} (arable soil) - 10^4 m g^{-1} (forest soil). Given a retention of phages to the mycelial surface of $R_P = 10^7$ PFU mm^{-2} and a presumed hyphal diameter of 10^{-5} m, such fungal biomass would translate to a calculated mycelial surface of $\approx 0.0031 – 0.3140$ m^2 or a hypothetical phage retention potential of 3×10^{10} to 3×10^{12} phages per gram of soil. This would correspond to 30 to 3000 times the reported average number of virus like particles per gram of soil,[78,79] and, hence, be an important location for phage retention. Some hyphae are also known to become hydrophobic,[50] when exposed to air in unsaturated soil conditions or during periods of soil drying. Hydrophobic mycelia may retain phages particularly well when exposed to conditions of soil water flow during major rain events. A recent 1-year time-series analysis of virus-like particle abundances in soils along a transect with different land-use practices, for instance, proposed rainfall-induced mobilization of viruses and correlations between rainfall and virus abundances in non-forest sites.[79] Furthermore, the physico-chemical effects of phage and hyphal

surface properties on phage retention to mycelia can influence the structure of soil; for instance, some hyphae exert polysaccharides and glycoprotein mucilages[39] that enable the aggregation of soil mineral particles and organic matter.[71] These aggregates play a crucial role in the retention of viruses due to exclusion effects at the pore-scale.[80] At the micrometer scale, fungi take advantage of the three-dimensional space in the soil.[48] Their small hyphal diameter, which is approximately 1/60th the thickness of roots, allows fungi to access tight spaces.[30] This promotes the possible role that hyphae may play in the transport of colloidal particles, as bonding forces tend to be stronger at smaller size scales.[39] Consequently, understanding phage-mycelial interactions may help in planning different environmental and health related applications. For instance, tracer phages, which exhibit less retention in the presence of fungal mycelia, will be better tracer phages for tracer studies in terrestrial ecosystems. On the other hand, fungal mycelia with high phage retention potential can be used in the design of filter systems to reduce or hinder the transport of undesirable entities, e.g., pathogenic viruses, bacteria or anthropogenic nanoparticles. Accordingly, investigations concerning the influence of mycelia on the retention of phages could be extended to nanoparticles, which will be of interest for different applications. Further, the retention of phages by mycelia may increase the phage accessibility to bacteria, influence the multifarious bacterial-fungal interactions ,[81,34] and/or promote phage-induced gene mobility in microbiomes of the mycosphere. Future work will need to include studies under more complex environmental conditions.

ACKNOWLEDGMENTS

This study is part of the Collaborative Research Centre AquaDiva (CRC 1076 AquaDiva) at the Friedrich Schiller University Jena and the Helmholtz Centre for Environmental Research - UFZ and was funded by the Deutsche Forschungsgemeinschaft (DFG). C.E.S. also acknowledges financial support by the Swiss National Science Foundation (Ambizione Grant No. PZ00P2_168005). The authors wish to thank Laura Sánchez Fontanet, Jana Reichenbach, Birgit Würz and Luisa Ciabarri for

skilled technical help as well as Bijing Xiong (UFZ) for the photograph of the microfluidic device used in Fig. 1C and the TOC. The authors further thank Tom Berthold, Anja Worrich and René Kallies for helpful discussions and Prof. M. Künzler (ETH Zürich) for kindly providing *C. cinerea* strain AmutBmut pMA412.

SUPPLEMENTARY MATERIAL

Supporting Information is available and contains three figures and two tables.

CONFLICT OF INTEREST

The authors declare that the research was conducted in the absence of any commercial or financial relationships that could be construed as a potential conflict of interest.

FIGURE LEGENDS

Figure 1. (A) Photograph of the microfluidic platform used to monitor phage-mycelial interactions. A mycelial inoculum was placed next to the lateral opening of the microfluidic device (made from poly(dimethylsiloxane) (PDMS) silicone elastomer), allowing hyphae to penetrate and grow into the observation channel via a constriction channel, as illustrated in the two-dimensional overview of the microchannel geometry (B). Hyphal growth was observed in the observation channel, as indicated by the red dotted frame in (B), using bright field or fluorescence microscopy. (C) A bright-field micrograph of *P. ultimum* hyphae (24 h post inoculation). (D) A fluorescence micrograph of *C. cinerea* hyphae (48 h post inoculation). The direction of hyphal growth was toward the outlet.

Figure 2. PSA-HS2 and T4 phage concentrations in the influent (light grey bars) and the effluent of the microfluidic devices in the absence (black) and presence (grey) of hyphae after 4 and 22 h of continuous flow (5 µL h^{-1}). Phages were enumerated by plaque forming units (PFU) depicted by total (primary y-axis on the left hand side of each panel). Data represent averages and standard deviations of triplicate experiments (except for duplicates for PSA-HS2 with *C. cinerea*). The asterisks on top of the columns refer to statistically significant differences (determined using two-tailed t-test) between the effluent concentration (in the presence of hyphae) and the corresponding controls (i.e. influent concentration and effluent concentration in the absence of hyphae): $p \leq 0.05$ (*), $p \leq 0.01$ (**) and $p \leq 0.001$ (***).

Figure 3. Total number of T4 or PSA-HS2 phages retained per mm^2 of the mycelial surface after 4 h of phage percolation through the microfluidic devices containing either hyphae of *P. ultimum* or C. *cinerea*. Data represent averages and standard deviations of triplicate experiments (except for

duplicates for PSA-HS2 & *C. cinerea*). Asterisks indicate significant differences, if present, between different phage and mycelia pairs: $p \leq 0.01$ (**) and $p \leq 0.001$ (***).

Figure 4. XDLVO interaction energy profiles between phages and mycelia. The interaction energy profiles show the overall interaction energy (GXDLVO; black solid line), the acid-base interaction energy (GAB; orange long-dashed line), the electrostatic repulsion (GEDL; blue short-dashed line), and the Lifshitz-van der Waals energy (GLW; red dotted-dashed line) as a function of distance particle h (nm) between the phage and the mycelia surface.

Table 1. Overview of the names, classifications, size and physico-chemical surface properties of the phages and hyphal organisms used in this study.

Name (Name of family or class)	**Phage host name**	**Zeta potential** ζ	**Water contact angle** Θ_w	**Size** (head/tail)	**Surface area**
		(mV)	(degree)	(µm)	(mm^2)
PSA-HS2 (*Siphoviridae*)	*Pseudoalteromonas* H13-15	-10 ± 1	40 ± 5 [a)]	0.21 [a)] (0.06/0.15) [a)]	--
T4 (*Myoviridae*)	*E. coli* (Migula 1895)	-10 ± 2	95 ± 5 [a)]	0.203 [a)] (0.09/0.113) [a)]	--
Pythium ultimum (*Oomycete*)	--	-11 ± 3	62 ± 6	10 ± 3 [b)]	1.2 ± 0.1 [c)]
Coprionopsis cinerea strain AmutBmut pMA412 (*Agaricomycete*)	--	-13 ± 4	131 ± 2	7 ± 1 [b)]	0.9 ± 0.4 [c)]

[a)] Data taken from Ghanem et al.[22] [b)] Average and standard deviations (n ≥ 20) of hyphal diameters, [c)] Average and standard deviations of the surface area of mycelia (n > 5) after 24 h (*P. ultimum*) and 48 h (*C. cinerea*) of inoculation.

Table 2. Calculated retention (RP) of phages to mycelial surfaces (0 - 4 h) and mass recoveries (*M*) of transport experiments in microfluidic devices, as well as the stability and viability of phage suspensions in the presence of *P. ultimum* and *C. cinerea* conditioned media. The values of the maximum energy barrier (Φ_{max1}), the primary minimum (Φ_{min1}), and the secondary minimum (Φ_{min2}) of phage-mycelia interaction energies were derived based on the XDLVO approach using a sphere-plate model.

Phage name	**Name of hyphal organisms**	**Retention of phages to mycelial surface (R_P) after 0 - 4 h** [a, b]	**Phage mass recovery with mycelia after 0 - 4 h (4 - 22 h)** [b]	**Phage mass recovery without mycelia after 0 - 4 h (4 - 22 h)** [b]	**Phage stability after 4 h (after 22 h)** [c]	**Calculated maximum energy barrier** [d]	**Calculated energy at primary minimum** [d]	**Calculated energy at secondary minimum** [d]
			M	*M*		Φ max1	Φ min1	Φ min2
		(PFU mm^{-2} ×10^6)	(%)	(%)	(%)	(k_BT ×10^{-3})	(k_BT ×10^4)	(k_BT ×10^{-3})
PSA-HS2	*Pythium ultimum*	4.26 ± 0.6	92 ± 3 (108 ± 12)	98 ± 5 (94 ± 0)	97 ± 23 (98 ± 16)	4.7	-1.1	-0.3
	Coprinopsis cinerea	13.6 ± 1.3	77 ± 2 (75 ± 6)	99 ± 0.2 (97 ± 0)	102 ± 11 (99 ± 16)	na [c]	-1.9	na [d]
T4	*Pythium ultimum*	2.3 ± 0.8	98 ± 4 (107 ± 15)	99 ± 1 (109 ± 7)	108 ± 6 (94 ± 3)	na [c]	-14	na [c]
	Coprinopsis cinerea	36.7 ± 0.61	7 ± 1 (86 ± 11)	98 ± 5 (92 ± 0.5)	106 ± 5 (86 ± 6)	na [c]	-29	na [c]

[a] Values are corrected for losses in the absence of mycelia (cf. eq. 2). [b] Influent concentrations of phages (PFU mL^{-1}): PSA-HS2 and *P. ultimum*: 1.7 × 10^9, PSA-HS2 and *C. cinerea*: 3.4 × 10^9, T4 and *P. ultimum*: 3.3 × 10^9; T4 and *C. cinerea*: 2.6 × 10^9 PFU mL^{-1}. [c] Phage stability in the presence of cell-free conditioned media. [d] As predicted by XDLVO interaction energy profiles (cf. eq. 3, Fig. 4). [e] No value could be calculated.

REFERENCES

(1) Paul, J. H.; Rose, J. B.; Brown, J.; Shinn, E. A.; Miller, S.; Farrah, S. R. Viral Tracer Studies Indicate Contamination of Marine Waters by Sewage Disposal Practices in Key Largo, Florida. *Appl. Environ. Microbiol.* **1995**, *61* (6), 2230–2234.

(2) Williamson, K. E.; Harris, J. V.; Green, J. C.; Rahman, F.; Chambers, R. M. Stormwater Runoff Drives Viral Community Composition Changes in Inland Freshwaters. *Front. Microbiol.* **2014**, *5*, 105. https://doi.org/10.3389/fmicb.2014.00105.

(3) Collins, K. E.; Cronin, A. A.; Rueedi, J.; Pedley, S.; Joyce, E.; Humble, P. J.; Tellam, J. H. Fate and Transport of Bacteriophage in UK Aquifers as Surrogates for Pathogenic Viruses. *Eng. Geol.* **2006**, *85* (1–2), 33–38. https://doi.org/10.1016/j.enggeo.2005.09.025.

(4) McKay, L. D.; Cherry, J. A.; Bales, R. C.; Yahya, M. T.; Gerba, C. P. A Field Example of Bacteriophage as Tracers of Fracture Flow. *Environ. Sci. Technol.* **1993**, *27* (6), 1075–1079.

(5) Flynn, R. M.; Mallèn, G.; Engel, M.; Ahmed, A.; Rossi, P. Characterizing Aquifer Heterogeneity Using Bacterial and Bacteriophage Tracers. *J. Environ. Qual.* **2015**, *44* (5), 1448. https://doi.org/10.2134/jeq2015.02.0117.

(6) Harvey, R. W.; Harms, H.; Landkamer, L. Transport of Microorganisms in the Terrestrial Subsurface: In Situ and Laboratory Methods. *Man. Environ. Microbiol.* **2002**, *2*, 753–776.

(7) Rossi, P. Advances in biological tracer techniques for hydrology and hydrogeology using bacteriophages, Université de Neuchâtel, 1994.

(8) Flynn, R.; Hunkeler, D.; Guerin, C.; Burn, C.; Rossi, P.; Aragno, M. Geochemical Influences on H40/1 Bacteriophage Inactivation in Glaciofluvial Sands. *Environ. Geol.* **2004**, *45* (4), 504–517.

(9) Goldscheider, N.; Haller, L.; Poté, J.; Wildi, W.; Zopfi, J. Characterizing Water Circulation and Contaminant Transport in Lake Geneva Using Bacteriophage Tracer Experiments and Limnological Methods. *Environ. Sci. Technol.* **2007**, *41* (15), 5252–5258. https://doi.org/10.1021/es070369p.

(10) Flynn, R. M.; Sinreich, M. Characterisation of Virus Transport and Attenuation in Epikarst Using Short Pulse and Prolonged Injection Multi-Tracer Testing. *Water Res.* **2010**, *44* (4), 1138–1149. https://doi.org/10.1016/j.watres.2009.11.032.

(11) Zhao, B.; Zhang, H.; Zhang, J.; Jin, Y. Virus Adsorption and Inactivation in Soil as Influenced by Autochthonous Microorganisms and Water Content. *Soil Biol. Biochem.* **2008**, *40* (3), 649–659. https://doi.org/10.1016/j.soilbio.2007.09.020.

(12) Moore, R. S.; Taylor, D. H.; Sturman, L. S.; Reddy, M. M.; Fuhs, G. W. Poliovirus Adsorption by 34 Minerals and Soils. *Appl. Environ. Microbiol.* **1981**, *42* (6), 963–975.

(13) Van Cuyk, S.; Siegrist, R. L. Virus Removal within a Soil Infiltration Zone as Affected by Effluent Composition, Application Rate, and Soil Type. *Water Res.* **2007**, *41* (3), 699–709. https://doi.org/10.1016/j.watres.2006.07.021.

(14) Kinoshita, T.; Bales, R. C.; Maguire, K. M.; Gerba, C. P. Effect of PH on Bacteriophage Transport through Sandy Soils. *J. Contam. Hydrol.* **1993**, *14* (1), 55–70. https://doi.org/10.1016/0169-7722(93)90041-P.

(15) Carlson, G. F.; Woodard, F. E.; Wentworth, D. F.; Sproul, O. J. Virus Inactivation on Clay Particles in Natural Waters. *J. Water Pollut. Control Fed.* **1968**, *40* (2), R89–R106.

(16) Taylor, D. H.; Moore, R. S.; Sturman, L. S. Influence of PH and Electrolyte Composition on Adsorption of Poliovirus by Soils and Minerals. *Appl. Environ. Microbiol.* **1981**, *42* (6), 976–984.

(17) Lance, J. C.; Gerba, C. P. Effect of Ionic Composition of Suspending Solution on Virus Adsorption by a Soil Column. *Appl. Environ. Microbiol.* **1984**, *47* (3), 484–488.

(18) Anders, R.; Chrysikopoulos, C. V. Transport of Viruses Through Saturated and Unsaturated Columns Packed with Sand. *Transp. Porous Media* **2009**, *76* (1), 121–138. https://doi.org/10.1007/s11242-008-9239-3.

(19) Trouwborst, T.; Kuyper, S.; De Jong, J. C.; Plantinga, A. D. Inactivation of Some Bacterial and Animal Viruses by Exposure to Liquid-Air Interfaces. *J. Gen. Virol.* **1974**, *24* (1), 155–165.

(20) Dika, C.; Duval, J. F. L.; Francius, G.; Perrin, A.; Gantzer, C. Isoelectric Point Is an Inadequate Descriptor of MS2, Phi X 174 and PRD1 Phages Adhesion on Abiotic Surfaces. *J. Colloid Interface Sci.* **2015**, *446*, 327–334. https://doi.org/10.1016/j.jcis.2014.08.055.

(21) Dowd, S. E.; Pillai, S. D.; Wang, S.; Corapcioglu, M. Y. Delineating the Specific Influence of Virus Isoelectric Point and Size on Virus Adsorption and Transport through Sandy Soils. *Appl. Environ. Microbiol.* **1998**, *64* (2), 405–410.

(22) Ghanem, N.; Kiesel, B.; Kallies, R.; Harms, H.; Chatzinotas, A.; Wick, L. Y. Marine Phages As Tracers: Effects of Size, Morphology, and Physico–Chemical Surface Properties on Transport in a Porous Medium. *Environ. Sci. Technol.* **2016**, *50* (23), 12816–12824. https://doi.org/10.1021/acs.est.6b04236.

(23) Küsel, K.; Totsche, K. U.; Trumbore, S. E.; Lehmann, R.; Steinhäuser, C.; Herrmann, M. How Deep Can Surface Signals Be Traced in the Critical Zone? Merging Biodiversity with Biogeochemistry Research in a Central German Muschelkalk Landscape. *Front. Earth Sci.* **2016**, *4*, 32. https://doi.org/10.3389/feart.2016.00032.

(24) John, D. E.; Rose, J. B. Review of Factors Affecting Microbial Survival in Groundwater. *Environ. Sci. Technol.* **2005**, *39* (19), 7345–7356. https://doi.org/10.1021/es047995w.

(25) Hurst, C. J. Influence of Aerobic Microorganisms upon Virus Survival in Soil. *Can. J. Microbiol.* **1988**, *34* (5), 696–699.

(26) Sobsey, M. D.; Dean, C. H.; Knuckles, M. E.; Wagner, R. A. Interactions and Survival of Enteric Viruses in Soil Materials. *Appl. Environ. Microbiol.* **1980**, *40* (1), 92–101.

(27) Campbell, R. N. Fungal Transmission of Plant Viruses. *Annu. Rev. Phytopathol.* **1996**, *34* (1), 87–108.

(28) Alfaro-Fernández, A.; Del Carmen Córdoba-Sellés, M.; Herrera-Vásquez, J. Á.; Cebrián, M. del C.; Jordá, C. Transmission of Pepino Mosaic Virus by the Fungal Vector Olpidium Virulentus. *J. Phytopathol.* **2010**, *158* (4), 217–226. https://doi.org/10.1111/j.1439-0434.2009.01605.x.

(29) Varanda, C. M. R.; Silva, M. S. M. R.; Félix, M. do R. F.; Clara, M. I. E. Evidence of Olive Mild Mosaic Virus Transmission by Olpidium Brassicae. *Eur. J. Plant Pathol.* **2011**, *130* (2), 165–172. https://doi.org/10.1007/s10658-011-9742-1.

(30) Pennisi, E. The Secret Life of Fungi. *Science* **2004**, *304* (5677), 1620.

(31) Kendrick, B. *The Fifth Kingdom*; Focus Pub., 2000.

(32) Kohlmeier, S.; Smits, T. H. M.; Ford, R. M.; Keel, C.; Harms, H.; Wick, L. Y. Taking the Fungal Highway: Mobilization of Pollutant-Degrading Bacteria by Fungi. *Environ. Sci. Technol.* **2005**, *39* (12), 4640–4646. https://doi.org/10.1021/es047979z.

(33) Harms, H.; Schlosser, D.; Wick, L. Y. Untapped Potential: Exploiting Fungi in Bioremediation of Hazardous Chemicals. *Nat. Rev. Microbiol.* **2011**, *9* (3), 177–192. https://doi.org/10.1038/nrmicro2519.

(34) Deveau, A.; Bonito, G.; Uehling, J.; Paoletti, M.; Becker, M.; Bindschedler, S.; Hacquard, S.; Hervé, V.; Labbé, J.; Lastovetsky, O. A.; Mieszkin, S.; Millet, L.J.; Vajna, B.; Junier, P.; Bonfante, P.; Krom, B.P.; Olsson, S.; van Elsas, J.D.; Wick, L.Y.. Bacterial-Fungal Interactions: Ecology, Mechanisms and Challenges. *FEMS Microbiol. Rev.* **2018**, *42* (3), 335–352. https://doi.org/10.1093/femsre/fuy008.

(35) Berthold, T.; Centler, F.; Hübschmann, T.; Remer, R.; Thullner, M.; Harms, H.; Wick, L. Y. Mycelia as a Focal Point for Horizontal Gene Transfer among Soil Bacteria. *Sci. Rep.* **2016**, *6*. https://doi.org/10.1038/srep36390.

(36) Zhang, M.; Silva, P. e; C, M. de; De Mares Maryam, C.; Elsas, V.; Dirk, J. The Mycosphere Constitutes an Arena for Horizontal Gene Transfer with Strong Evolutionary Implications for Bacterial-Fungal Interactions. *FEMS Microbiol. Ecol.* **2014**, *89* (3), 516–526. https://doi.org/10.1111/1574-6941.12350.

(37) Wösten, H. A. B.; van Wetter, M.-A.; Lugones, L. G.; van der Mei, H. C.; Busscher, H. J.; Wessels, J. G. H. How a Fungus Escapes the Water to Grow into the Air. *Curr. Biol.* **1999**, *9* (2), 85–88. https://doi.org/10.1016/S0960-9822(99)80019-0.

(38) Smits, M. M.; Herrmann, A. M.; Duane, M.; Duckworth, O. W.; Bonneville, S.; Benning, L. G.; Lundström, U. The Fungal–mineral Interface: Challenges and Considerations of Micro-Analytical Developments. *Fungal Biol. Rev.* **2009**, *23* (4), 122–131. https://doi.org/10.1016/j.fbr.2009.11.001.

(39) Ritz, K.; Young, I. M. Interactions between Soil Structure and Fungi. *Mycologist* **2004**, *18* (2), 52–59.

(40) Deng, L.; Gregory, A.; Yilmaz, S.; Poulos, B. T.; Hugenholtz, P.; Sullivan, M. B. Contrasting Life Strategies of Viruses That Infect Photo- and Heterotrophic Bacteria, as Revealed by Viral Tagging. *mBio* **2012**, *3* (6), e00373-12-e00373-12. https://doi.org/10.1128/mBio.00373-12.

(41) Clokie, M. R.; Millard, A. D.; Letarov, A. V.; Heaphy, S. Phages in Nature. *Bacteriophage* **2011**, *1* (1), 31–45.

(42) Hijnen, W. A. M.; Brouwer-Hanzens, A. J.; Charles, K. J.; Medema, G. J. Transport of MS2 Phage, *Escherichia Coli, Clostridium Perfringens* , *Cryptosporidium Parvum,* and *Giardia Intestinalis* in a Gravel and a Sandy Soil. *Environ. Sci. Technol.* **2005**, *39* (20), 7860–7868. https://doi.org/10.1021/es050427b.

(43) Mohn, G.; Ellenberger, J.; McGregor, D. Development of Mutagenicity Test Using Escherichia Coli K-12 as Indicator Organism. *Mutat. Res.* **1974**, *25* (2), 187–196.

(44) Duhaime, M. B.; Solonenko, N.; Roux, S.; Verberkmoes, N. C.; Wichels, A.; Sullivan, M. B. Comparative Omics and Trait Analyses of Marine Pseudoalteromonas Phages Advance the Phage OTU Concept. *Front. Microbiol.* **2017**, *8*. https://doi.org/10.3389/fmicb.2017.01241.

(45) Oppenheimer, C.; Zobell, C. The Growth and Viability of 63 Species of Marine Bacteria as Influenced. *J. Mar. Res.* **1952**, *11* (1), 10–18.

(46) Sezonov, G.; Joseleau-Petit, D.; D'Ari, R. Escherichia Coli Physiology in Luria-Bertani Broth. *J. Bacteriol.* **2007**, *189* (23), 8746–8749. https://doi.org/10.1128/JB.01368-07.

(47) Stanley, C. E.; Stöckli, M.; Swaay, D. van; Sabotič, J.; Kallio, P. T.; Künzler, M.; deMello, A. J.; Aebi, M. Probing Bacterial–fungal Interactions at the Single Cell Level. *Integr. Biol.* **2014**, *6* (10), 935–945. https://doi.org/10.1039/C4IB00154K.

(48) Furuno, S.; Päzolt, K.; Rabe, C.; Neu, T. R.; Harms, H.; Wick, L. Y. Fungal Mycelia Allow Chemotactic Dispersal of Polycyclic Aromatic Hydrocarbon-Degrading Bacteria in Water-Unsaturated Systems. *Environ. Microbiol.* **2010**, *12* (6), 1391–1398. https://doi.org/10.1111/j.1462-2920.2009.02022.x.

(49) Thompson, S. S.; Flury, M.; Yates, M. V.; Jury, W. A. Role of the Air-Water-Solid Interface in Bacteriophage Sorption Experiments. *Appl. Environ. Microbiol.* **1998**, *64* (1), 304–309.

(50) Smits, T. H. M.; Wick, L. Y.; Harms, H.; Keel, C. Characterization of the Surface Hydrophobicity of Filamentous Fungi. *Environ. Microbiol.* **2003**, *5* (2), 85–91.

(51) Stanley, C.; Shrivastava, J.; Brugman, R.; Heinzelmann, E.; Frajs, V.; Bühler, A.; van Swaay, D.; Grossmann, G. Fabrication and Use of the Dual-Flow-RootChip for the Imaging of Arabidopsis Roots in Asymmetric Microenvironments. *BIO-Protoc.* **2018**, *8* (18). https://doi.org/10.21769/BioProtoc.3010.

(52) Schneider, C. A.; Rasband, W. S.; Eliceiri, K. W. NIH Image to ImageJ: 25 Years of Image Analysis. *Nat. Methods* **2012**, *9* (7), 671.

(53) Jensen, E. C. Quantitative Analysis of Histological Staining and Fluorescence Using ImageJ. *Anat. Rec.* **2013**, *296* (3), 378–381. https://doi.org/10.1002/ar.22641.

(54) Syngouna, V. I.; Chrysikopoulos, C. V. Transport of Biocolloids in Water Saturated Columns Packed with Sand: Effect of Grain Size and Pore Water Velocity. *J. Contam. Hydrol.* **2011**, *126* (3–4), 301–314. https://doi.org/10.1016/j.jconhyd.2011.09.007.

(55) Boks, N. P.; Norde, W.; van der Mei, H. C.; Busscher, H. J. Forces Involved in Bacterial Adhesion to Hydrophilic and Hydrophobic Surfaces. *Microbiology* **2008**, *154* (10), 3122–3133. https://doi.org/10.1099/mic.0.2008/018622-0.

(56) Bergendahl, J.; Grasso, D. Prediction of Colloid Detachment in a Model Porous Media: Thermodynamics. *AIChE J.* **1999**, *45* (3), 475–484. https://doi.org/10.1002/aic.690450305.

(57) Chrysikopoulos, C. V.; Syngouna, V. I. Attachment of Bacteriophages MS2 and _X174 onto Kaolinite and Montmorillonite: Extended-DLVO Interactions. *Colloids Surf. B Biointerfaces* **2012**, *92*, 74–83. https://doi.org/10.1016/j.colsurfb.2011.11.028.

(58) van Oss, C. J.; Docoslis, A.; Wu, W.; Giese, R. F. Influence of Macroscopic and Microscopic Interactions on Kinetic Rate Constants: I. Role of the Extended DLVO Theory in Determining the Kinetic Adsorption Constant of Proteins in Aqueous Media, Using von Smoluchowski's Approach. *Colloids Surf. B Biointerfaces* **1999**, *14* (1–4), 99–104. https://doi.org/10.1016/S0927-7765(99)00028-4.

(59) Mulligan, A. E.; Charette, M. A. Groundwater Flow to the Coastal Ocean. In *Encyclopedia of Ocean Sciences (Second Edition)*; Steele, J. H., Ed.; Academic Press: Oxford, 2009; pp 88–97. https://doi.org/10.1016/B978-012374473-9.00645-7.

(60) Hermansson, M. The DLVO Theory in Microbial Adhesion. *Colloids Surf. B Biointerfaces* **1999**, *14* (1), 105–119.

(61) van Loosdrecht, M. C.; Lyklema, J.; Norde, W.; Zehnder, A. J. Bacterial Adhesion: A Physicochemical Approach. *Microb. Ecol.* **1989**, *17* (1), 1–15.

(62) Jucker, B. A. Polymer Interactions and Bacterial Adhesion. PhD Thesis, ETH Zurich, 1998.

(63) Hahn, M. W.; O'Melia, C. R. Deposition and Reentrainment of Brownian Particles in Porous Media under Unfavorable Chemical Conditions: Some Concepts and Applications. *Environ. Sci. Technol.* **2004**, *38* (1), 210–220. https://doi.org/10.1021/es030416n.

(64) Shen, C.; Li, B.; Huang, Y.; Jin, Y. Kinetics of Coupled Primary- and Secondary-Minimum Deposition of Colloids under Unfavorable Chemical Conditions. *Environ. Sci. Technol.* **2007**, *41* (20), 6976–6982. https://doi.org/10.1021/es070210c.

(65) Stanley, C. E.; Grossmann, G.; Solvas, X. C. i; deMello, A. J. Soil-on-a-Chip: Microfluidic Platforms for Environmental Organismal Studies. *Lab. Chip* **2016**, *16* (2), 228–241. https://doi.org/10.1039/C5LC01285F.

(66) Stanley, C. E.; Heijden, M. G. A. van der. Microbiome-on-a-Chip: New Frontiers in Plant–Microbiota Research. *Trends Microbiol.* **2017**, *25* (8), 610–613. https://doi.org/10.1016/j.tim.2017.05.001.

(67) Attinti, R.; Wei, J.; Kniel, K.; Sims, J. T.; Jin, Y. Virus' (MS2, ΦX174, and Aichi) Attachment on Sand Measured by Atomic Force Microscopy and Their Transport through Sand Columns. *Environ. Sci. Technol.* **2010**, *44* (7), 2426–2432. https://doi.org/10.1021/es903221p.

(68) Dika, C.; Ly-Chatain, M. H.; Francius, G.; Duval, J. F. L.; Gantzer, C. Non-DLVO Adhesion of F-Specific RNA Bacteriophages to Abiotic Surfaces: Importance of Surface Roughness, Hydrophobic and Electrostatic Interactions. *Colloids Surf. Physicochem. Eng. Asp.* **2013**, *435*, 178–187. https://doi.org/10.1016/j.colsurfa.2013.02.045.

(69) You, Y.; Vance, G. F.; Sparks, D. L.; Zhuang, J.; Jin, Y. Sorption of MS2 Bacteriophage to Layered Double Hydroxides. *J. Environ. Qual.* **2003**, *32* (6), 2046–2053.

(70) Schijven, J. F.; Hassanizadeh, S. M. Removal of Viruses by Soil Passage: Overview of Modeling, Processes, and Parameters. *Crit. Rev. Environ. Sci. Technol.* **2000**, *30* (1), 49–127. https://doi.org/10.1080/10643380091184174.

(71) Bardgett, R. *The Biology of Soil: A Community and Ecosystem Approach*; Biology of Habitats Series; Oxford University Press: Oxford, New York, 2005.

(72) Chrysikopoulos, C. V.; Aravantinou, A. F. Virus Inactivation in the Presence of Quartz Sand under Static and Dynamic Batch Conditions at Different Temperatures. *J. Hazard. Mater.* **2012**, *233–234*, 148–157. https://doi.org/10.1016/j.jhazmat.2012.07.002.

(73) Pecson, B. M.; Decrey, L.; Kohn, T. Photoinactivation of Virus on Iron-Oxide Coated Sand: Enhancing Inactivation in Sunlit Waters. *Water Res.* **2012**, *46* (6), 1763–1770. https://doi.org/10.1016/j.watres.2011.12.059.

(74) Totsche, K. U.; Jann, S.; Kögel-Knabner, I. Single Event–Driven Export of Polycyclic Aromatic Hydrocarbons and Suspended Matter from Coal Tar–Contaminated Soil. *Vadose Zone J.* **2007**, *6* (2), 233–243. https://doi.org/10.2136/vzj2006.0083.

(75) Worrich, A.; Wick, L. Y.; Banitz, T. Chapter Three - Ecology of Contaminant Biotransformation in the Mycosphere: Role of Transport Processes. In *Advances in Applied Microbiology*; Gadd, G. M., Sariaslani, S., Eds.; Academic Press, 2018; Vol. 104, pp 93–133. https://doi.org/10.1016/bs.aambs.2018.05.005.

(76) Fester, T.; Giebler, J.; Wick, L. Y.; Schlosser, D.; Kästner, M. Plant–microbe Interactions as Drivers of Ecosystem Functions Relevant for the Biodegradation of Organic Contaminants. *Curr. Opin. Biotechnol.* **2014**, *27*, 168–175. https://doi.org/10.1016/j.copbio.2014.01.017.

(77) Otten, W.; Hall, D.; Harris, K.; Ritz, K.; Young, I. M.; Gilligan, C. A. Soil Physics, Fungal Epidemiology and the Spread of Rhizoctonia Solani. *New Phytol.* **2001**, *151* (2), 459–468. https://doi.org/10.1046/j.0028-646x.2001.00190.x.

(78) Williamson, K. E.; Radosevich, M.; Wommack, K. E. Abundance and Diversity of Viruses in Six Delaware Soils. *Appl. Environ. Microbiol.* **2005**, *71* (6), 3119–3125. https://doi.org/10.1128/AEM.71.6.3119-3125.2005.

(79) Narr, A.; Nawaz, A.; Wick, L. Y.; Harms, H.; Chatzinotas, A. Soil Viral Communities Vary Temporally and along a Land Use Transect as Revealed by Virus-Like Particle Counting and a Modified Community Fingerprinting Approach (FRAPD). *Front. Microbiol.* **2017**, *8*. https://doi.org/10.3389/fmicb.2017.01975.

(80) Sirivithayapakorn, S.; Keller, A. Transport of Colloids in Saturated Porous Media: A Pore-Scale Observation of the Size Exclusion Effect and Colloid Acceleration. *Water Resour. Res.* **2003**, *39* (4), n/a-n/a. https://doi.org/10.1029/2002WR001583.

(81) Worrich, A.; Wick, L. Y.; Banitz, T. Ecology of Contaminant Biotransformation in the Mycosphere: Role of Transport Processes. *Adv. Appl. Microbiol.* **2018**, *104*, 93–133. https://doi.org/10.1016/bs.aambs.2018.05.005.

(82) Pratama, A. A. and van Elsas J. D.; Gene mobility in microbiomes of the mycosphere and mycorrhizosphere –role of plasmids and bacteriophages. *FEMS Microbiol. Ecol.* **2019**, *95*, Issue 5, fiz053, https://doi.org/10.1093/femsec/fiz053.

FIGURES

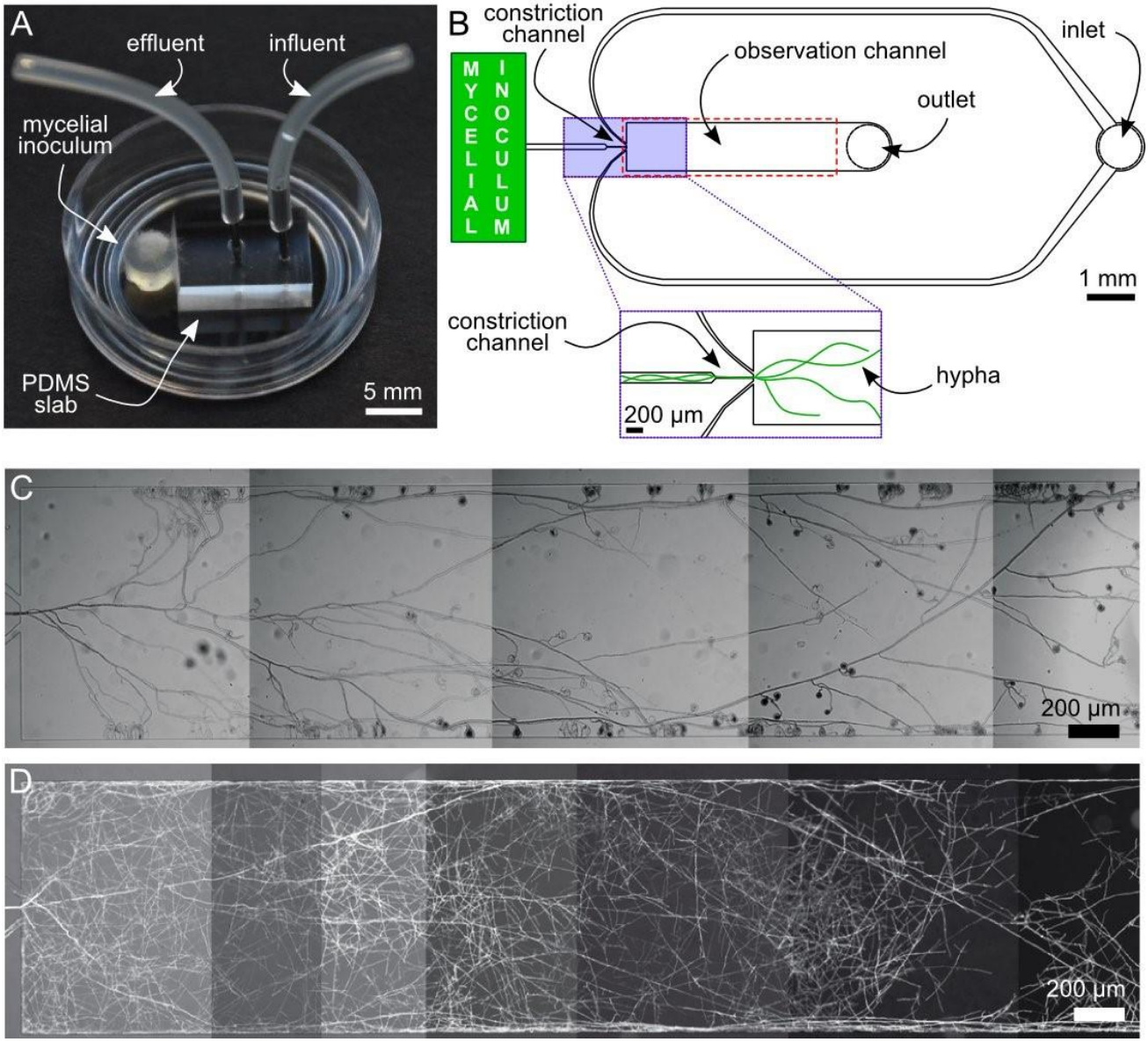

Figure 1

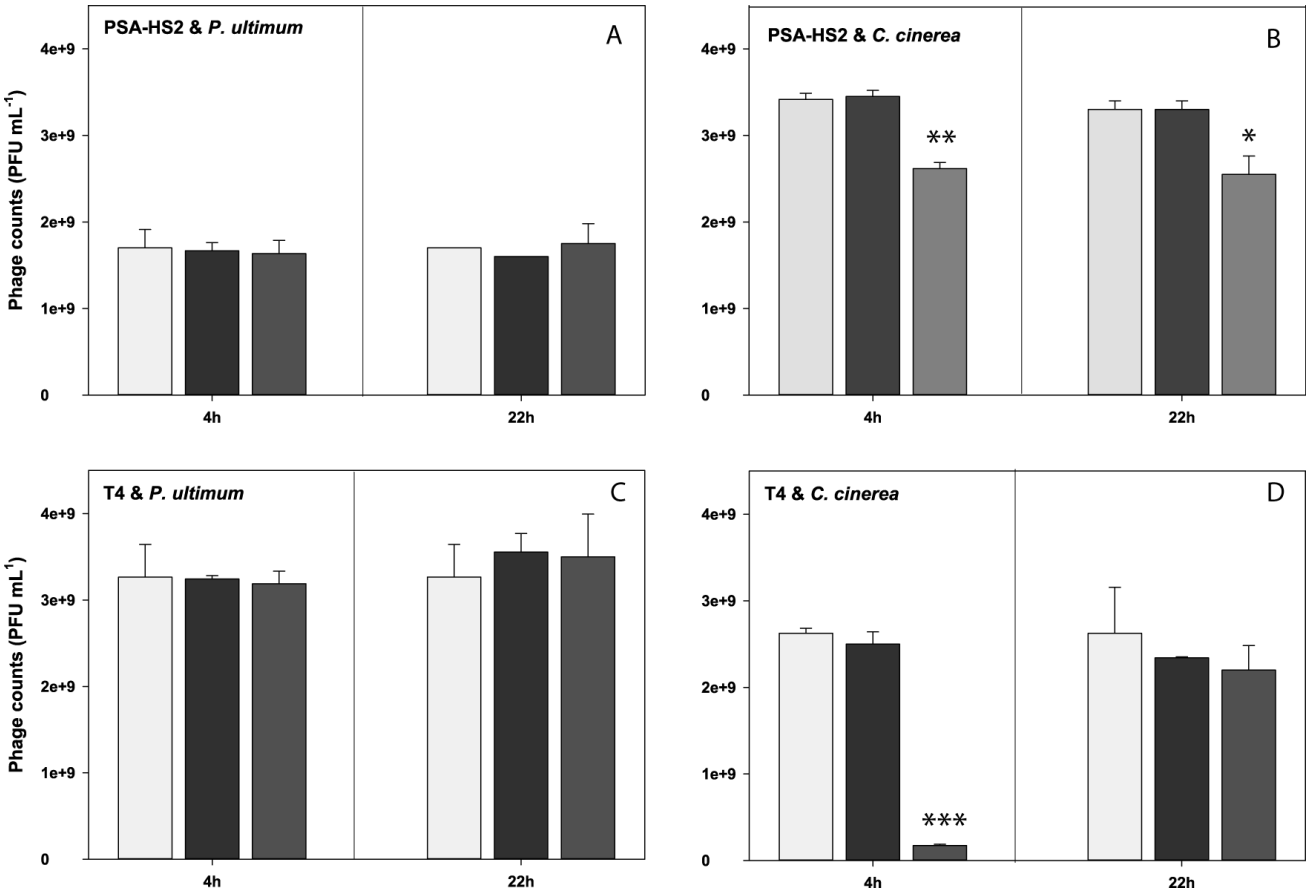
PSA-HS2 & P. ultimum
A
PSA-HS2 & C. cinerea
B
T4 & P. ultimum
C
T4 & C. cinerea
D
Phage counts (PFU mL-1)
4e+9
3e+9
2e+9
1e+9
0
4h
22h
**
*
***

Figure 2

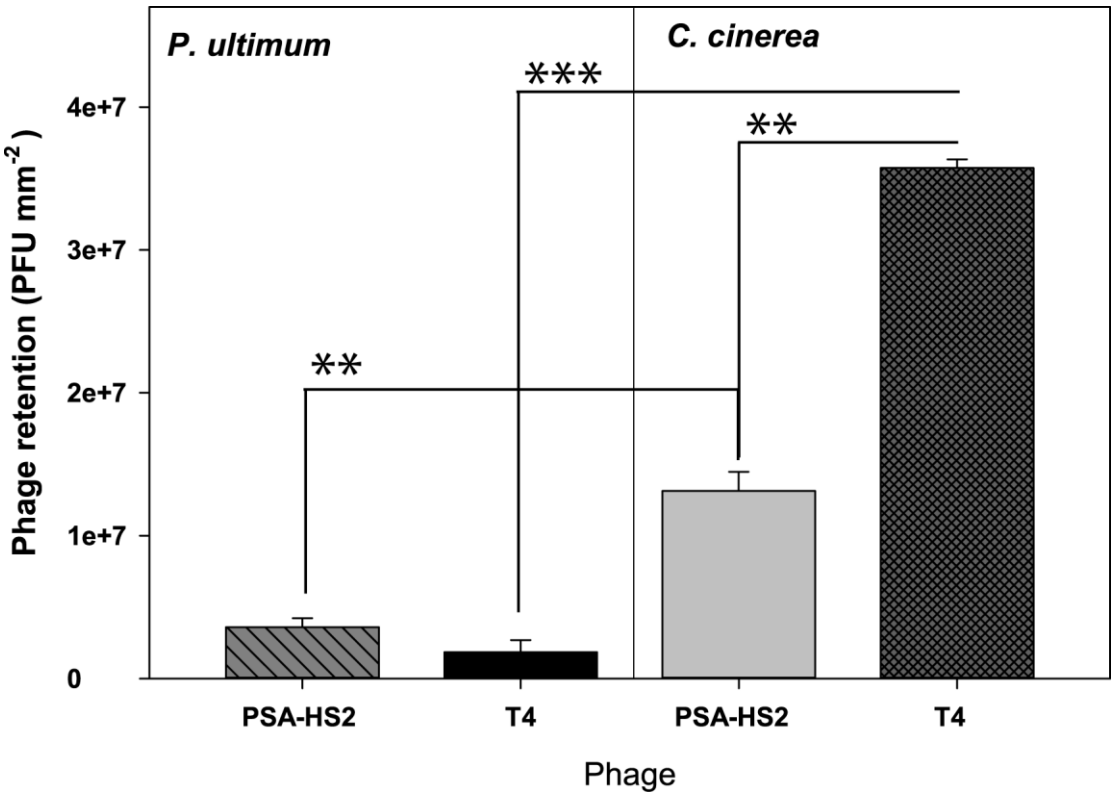
P. ultimum
C. cinerea
***
**
**
4e+7
3e+7
2e+7
1e+7
0
Phage retention (PFU mm-2)
PSA-HS2
T4
PSA-HS2
T4
Phage

Figure 3

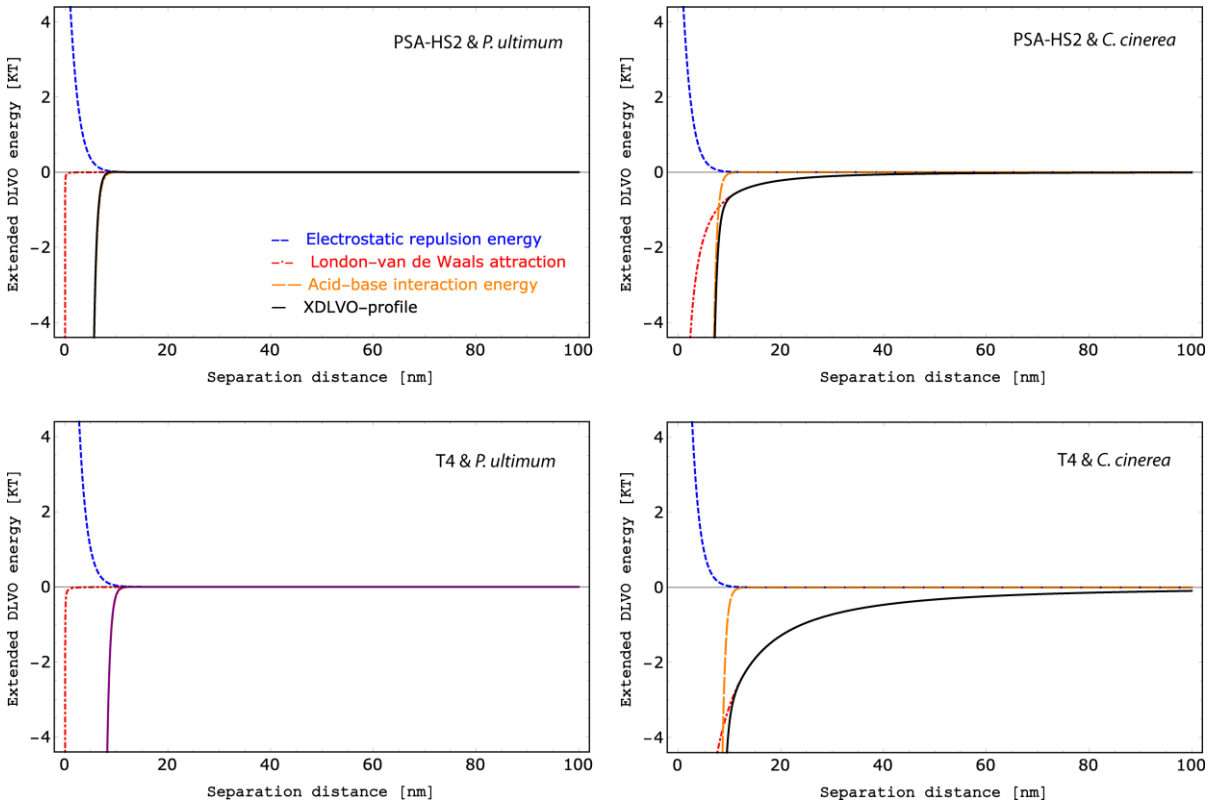

712

713

714 **Figure 4**

715

716

Supporting information

MYCELIAL EFFECTS ON PHAGE RETENTION DURING TRANSPORT IN A MICROFLUIDIC PLATFORM

Nawras Ghanem[1], Claire E. Stanley[2], Hauke Harms[1,3], Antonis Chatzinotas[1,3] and Lukas Y. Wick[1*]

[1]*Helmholtz Centre for Environmental Research - UFZ, Department of Environmental Microbiology, Permoserstraße 15, 04318 Leipzig, Germany.*

[2]*Agroecology and Environment Research Division, Agroscope, Reckenholzstrasse 191, 8046 Zurich, Switzerland*

[3]*German Centre for Integrative Biodiversity Research (iDiv) Halle-Jena-Leipzig, Deutscher Platz 5e, 04103 Leipzig, Germany*

Number of pages: 14

Number of figures: 2

Number of tables: 2

[*] Corresponding author: Mailing address: Helmholtz Centre for Environmental Research - UFZ. Department of Environmental Microbiology; Permoserstrasse 15; 04318 Leipzig, Germany. phone: +49 341 235 1316, fax: +49 341 235 45 1316, e-mail: lukas.wick@ufz.de.

MICROFLUIDIC DEVICE DESIGN AND PREPARATION

Microfluidic devices were prepared as described in Stanley et al.[1] In brief: A polyester film photolithography mask (Micro Lithography Services Ltd., UK) and a 100 mm silicon wafer (Silicon Materials, Germany), spin-coated with a 10 µm thick layer of SU-8 photoresist (MicroChem, USA), were used to create the master mold. The channel architecture was based on the fluid exchange device, detailed in Stanley et al.,[2] and enables active pumping of solutions into the observation chamber (Fig. 1). Two versions of the design were made, one that allows a mycelium to occupy the observation chamber and one that does not (Fig. S3). The latter design enables control measurements to be performed (i.e., in the absence of a mycelium). Polydimethylsiloxane (PDMS) silicone elastomer was then prepared and poured onto the master mold. PDMS was prepared using a 10:1 ratio of base to curing agent (Sylgard 184, Dow Corning, USA) that was mixed thoroughly and degassed prior to pouring. After curing overnight at 70 °C, the PDMS was removed from the mold and diced into slabs. A precision cutter (Syneo, USA), having a cutting edge diameter of 1.02 mm, was used to punch the holes for the medium inlet and outlet as illustrated in Fig. 1 and Fig. S3. The PDMS slabs were washed in 0.5 M sodium hydroxide, 70 % v/v ethanol, and sterile double distilled water (ddH2O) and then dried at 70 °C for 1 h. They were then bonded to glass-bottomed Petri dishes (World Precision Instruments) and sterilized for 20 minutes under ultraviolet light.

Fluorinated ethylene polymer (FEP) tubing (inner diameter: 0.80 mm, outer diameter: 1.60 mm; Cole-Parmer, Germany), hollow steel pin connectors (20 ga; Instech Laboratories, USA) and connector pins fitted with a luer-lock adaptor (20 ga; Instech Laboratories, USA) were used to connect the syringe to the microfluidic device and subsequently allow a variety of test solutions to be introduced into the observation channel (in the presence or absence of a mycelium). Fig. 1 shows an overview of the microfluidic setup for clarity.

MICROFLUIDIC DEVICE: CHARACTERIZATION OF FLOW CONDITIONS

The microfluidic device (channel height: 10 µm; channel width: 1000 µm; channel length: 6 mm) operates at laminar flow conditions (i.e. is a laminar flow reactor) with a Reynold's number (Re) equal to ca. 0.003 (eq. S1).

$$Re = \frac{QD_H}{vA} = \frac{1.4 \times 10^{-12}\, m^3/s \times 2 \times 10^{-5} m}{1 \times 10^{-6} m^2/s \times 1 \times 10^{-8} m^2} = \frac{2.8 \times 10^{-17} m^4/s}{1.0 \times 10^{-14} m^4/s} = 0.003 \quad \text{(S1)}$$

where:

Q = volumetric flow rate (m^3/s); i.e.: Q = 5 µL h^{-1} = 5 × 10^{-6} L h^{-1} = 1.4 × 10^{-12} (m^3 s^{-1})

D_H = hydraulic diameter (m), $D_H = \frac{4 \times cross\ sectional\ area}{wetted\ perimeter} = \frac{4 \times 10000}{2020} \frac{\mu m^2}{\mu m} = 20\ \mu m = 2 \times 10^{-5} m$

V = kinematic viscosity (m^2/s); i.e. 1.0 × 10^{-6} m^2/s (for water)

A = cross sectional area (m^2); i.e. 10,000 μm^2 = 1.0 × 10^{-8} m^2

A syringe pump ensured that the volumetric flow rate in the microchannels is controlled by adjusting the pressure needed to produce the required flow rate independent of channel geometry.[3] As the microchannels within this microfluidic device have a rectangular profile (with a high width: height ratio, i.e. 1000/10 = 100), the velocity distribution profile across the microchannel is highly uniform.[4]

Hence, taking the average velocity of the system to be 1.4×10^{-4} m s^{-1} (average velocity = volumetric flow rate / cross section area), we estimate that it would take ca. 43 seconds for the fluid to reach the outflow (i.e. to traverse the entire observation chamber) assuming a channel length of 6×10^{-3} m.

CALCULATION OF THE XDLVO INTERACTION ENERGIES OF PHAGE DEPOSITION

The phage-mycelia interaction energy (G_{XDLVO} (h)) at a distance h (nm) between two surfaces was calculated using the extended DLVO (XDLVO) theory (cf. eq. S2) based on the sphere-plate model.[5] The XDLVO theory thereby is an extension of the DLVO approach, which is the sum of G_{EDL}, G_{LW} and the Born repulsion energy G_{Born}. In the XDLVO theory, the energy G_{XDLVO} (h) is composed of the electrostatic repulsion (G_{EDL}), the Lifshitz-van der Waals (G_{LW})[6] and the acid−base (G_{AB}) interaction energy (eq. S2).[5]

$$G_{\mathrm{XDLVO}}(h) = G_{\mathrm{AB}} + G_{\mathrm{EDL}}(h) + G_{\mathrm{LW}}(h) \quad \text{(S2)}$$

The DLVO approach does not consider the polar forces that are supposed to be dominant forces between particles in polar media.[7] Additionally, the acid-base (G_{AB}) interaction energy was reported in many studies to be essential in explaining the interaction behavior between approached particles.[5,8]

Acid-base interaction energy (G_{AB})

Eq. S3 was applied to calculate the acid-base interaction energy (G_{AB}):[9,5]

$$G_{AB}(h) = 2\pi a_P \Delta G^{AB} \lambda \exp\left(\frac{l_0 - h}{\lambda}\right) \quad \text{(S3)}$$

Where a_P is the radius of phages, and h is the separation distance between the phage and the mycelial surface. The λ is the characteristic decay length of AB interaction in water (estimated to be 0.6 nm).[10] The acid-base interaction energy depends on the Gibbs free energy of the phage and the fungus as given by eq. S3. ΔG^{AB} is the acid-base component of the free energy interaction at contact given by eq. S4:[10,7]

$$\Delta G^{AB} = [2\left(\sqrt{\gamma_P^+} - \sqrt{\gamma_F^+}\right)\left(\sqrt{\gamma_P^-} - \sqrt{\gamma_F^-}\right) - \left(\sqrt{\gamma_P^+} - \sqrt{\gamma_l^+}\right)\left(\sqrt{\gamma_P^-} - \sqrt{\gamma_l^-}\right) - \left(\sqrt{\gamma_F^+} - \sqrt{\gamma_l^+}\right)\left(\sqrt{\gamma_F^-} - \sqrt{\gamma_l^-}\right)] \quad \text{(S4)}$$

The surface Gibbs free energy of phage γ_P and the fungal γ_F surfaces (mJ m^{-2}) were calculated based on the measured contact angles (θ) of phages, membrane filters and fungal surfaces using water, formamide and methylene iodide as liquids by applying the Young equation according to eq. S5:

$$cos(\theta) = -1 + 2\frac{\sqrt{\gamma_P^{LW}\gamma_l^{LW}}}{\gamma_l^{total}} + 2\frac{\sqrt{\gamma_P^{+}\gamma_l^{-}}}{\gamma_l^{total}} + 2\frac{\sqrt{\gamma_P^{-}\gamma_l^{+}}}{\gamma_l^{total}} \quad \text{(S5)}$$

The total surface Gibbs free energy (γ^{total}) is separated in a Lifshitz-van der Waals (γ^{LW}) and an acid-base component (γ^{AB}) and is represented by eq. S6. The electron acceptor and the electron donor components of acid-base surface energy γ^+ and γ^- is shown in eq. S7.

$$\gamma^{total} = \gamma^{AB} + \gamma^{LW} \quad \text{(S6)}$$

$$\gamma_i^{AB} = 2\sqrt{\gamma_i^{+}\gamma_i^{-}} \quad \text{(S7)}$$

Following van Oss et al.[11] we calculated the phage parameters γ_p, γ_p^{LW}, γ_p^{+}, γ_p^{-}, while literature data was utilized for water, formamide and methyleneiodide.[12]

Electrostatic repulsion energy (G_{EDL})

Eq. S8 was applied to calculate the electrostatic repulsion energy between phages and the fungal surface:[13]

$$G_{EDL} = \pi\varepsilon_0\varepsilon_r a_p\{2\zeta_p\zeta_F \ln\left[\frac{1+\exp(-\kappa h)}{1-\exp(-\kappa h)}\right] + (\zeta_p^2 + \zeta_F^2)\ln[1-\exp(-2\kappa h)] \quad \text{(S8)}$$

where κ^{-1} is the thickness of the electrical double layer (EDL, nm) as calculated by the Guoy-Chapman theory with C and z being the molar bulk concentration and the charge number of the electrolytes, respectively (eq. S9).

$$\kappa^{-1} = [3.29zC^{1/2}]^{-1} \quad \text{(S9)}$$

For a 100 mM buffer solution a κ^{-1} of 0.65 nm was calculated.[12]

Lifshitz-van der Waals interaction energy (G_{LW})

Using the values of the effective Hamaker constant (eq. S11), the Lifshitz-van der Waals interaction energy can be approximated by eq. S10:[7,12]

$$G_{LW} = -\frac{A_{132}}{6}\left[\frac{2a_p(h+a_p)}{h(h+a_p)} - \ln\left(\frac{h+2a_p}{h}\right)\right] \quad \text{(S10)}$$

The Hamaker constant A_{132} is described by eq. S11:[14]

$$A_{123} = \left(\sqrt{A_{11}} - \sqrt{A_{33}}\right)\left(\sqrt{A_{22}} - \sqrt{A_{33}}\right) \quad \text{(S11)}$$

Here, A_{ii} denotes the individual Hamaker constant for phages (A_{11}), hyphae (A_{22},) and water (A_{33}). A_{33} was taken from the literature,[14] while A_{11} and A_{22} were calculated by eq. S12.

$$A_{ii} = 6\pi l_0^{\,2} \gamma_i^{LW} \quad \text{(S12)}$$

According to Fowkes,[15] the value of $6\pi l_0^{\,2}$ equals 1.44×10^{-18} m^2, with l_0 being the equilibrium separation distance between the phage and the fungus (0.157 nm).[11]

Table S1. Overview of the surface Gibbs free energy (γ) and the contact angles of water (θ_w), formamide (θ_f) and methylene iodide (θ_m) for the phages and hyphae studied.

Name	**Contact angle (Θ)**			**Surface free energy (mJ m^{-2})[1]**				
	Θ_w	Θ_f	Θ_m	γ^-	γ^+	γ^{AB}	γ^{LW}	γ^{Tot}
water	-	-	-	25.5*	25.50*	51.0*	21.8*	72.8*
formamide	-	-	-	39.6*	2.30*	19.0*	39.0*	58.0*
methylene iodide	-	-	-	< 0.1*	< 0.1*	≈ 0*	50.8*	50.8*
membrane filter Anodisc 25	23	-	-	-	-	-	-	-
T4	95	61	40	0.1	0.30	0.2	39.5	39.7
PSA-HS2	40	31	43	34.6	0.96	11.5	38.0	49.5
Pythium ultimum	62	47	72	17.3	4.49	17.6	21.8	39.4
Coprinopsis cinerea	131	106	131	0.0	4.47	0.2	1.5	1.7

* Surface free energy data for water, formamide and methylene iodide taken from.[12]

Table S2. Composition of the YMG and CCMM media use for *C. cinerea*.[1]

Medium	**Composition**
Yeast-malt extract-glucose (YMG) medium	0.4 % w/v yeast extract, 1 % w/v malt extract, 0.4 % w/v glucose, 1.5 % w/v agar
C. cinerea minimal medium (CCMM)	5 g L^{-1} glucose, 2 g L^{-1} asparagine, 50 mg L^{-1} adenine sulfate, 1 g L^{-1} KH_2PO_4 , 2.25 g L^{-1} Na_2HPO_4, 0.29 g L^{-1} Na_2SO_4, 0.5 g L^{-1} 2di-ammonium tartrate, 0.04 mg L^{-1} thiamine hydrochloride, 0.25 g L^{-1} $MgSO_4$, 5 mg L^{-1} *p*-aminobenzoic acid (pABA).

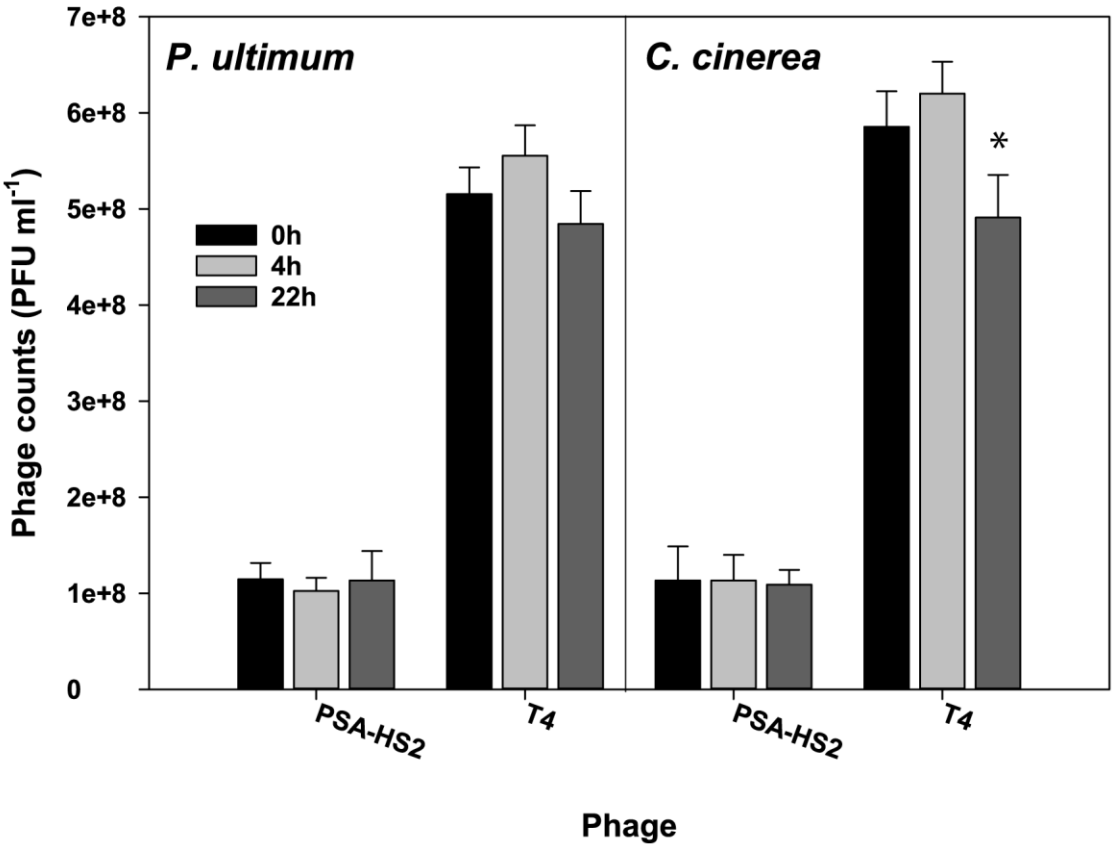

Figure S1. Stability and viability of the PSA-HS2 and T4 phage suspensions after exposure to *P. ultimum* and *C. cinerea* conditioned media (at t = 0, 4 and 22 h). The results represent the average and standard deviations of triplicate experiments using phage quantification by PFU. T4 counts in the presence of *C. cinerea* conditioned medium at t = 22 h were statistically different to initial concentrations at t = 0 and t = 4 h, as indicated by the asterisk ($p \leq 0.05$).

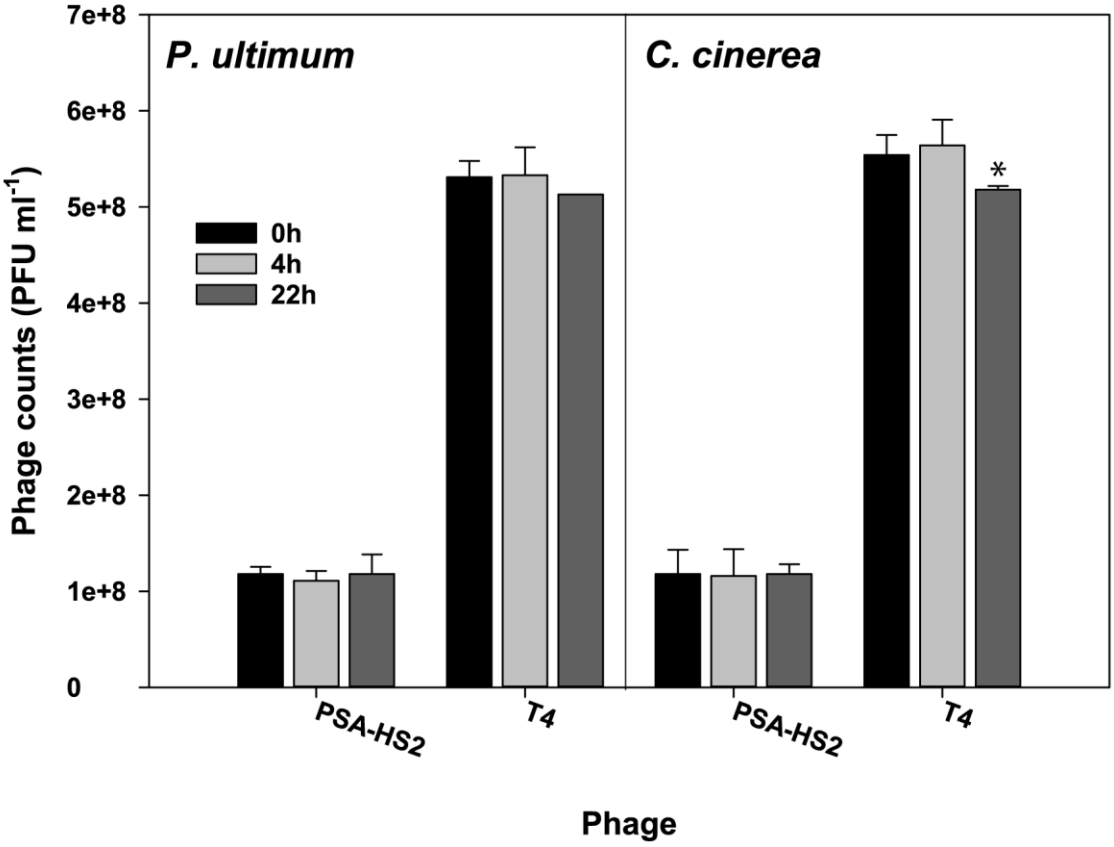

Figure S2. Stability and viability of the PSA-HS2 and T4 phage suspensions after exposure to fresh media i.e. LB and CCMM media for *P. ultimum* and *C. cinerea*, respectively at t = 0, 4 and 22 h. The results represent the average and standard deviations of triplicate experiments using phage quantification by PFU. T4 counts in the presence of *C. cinerea* conditioned medium at t = 22 h were statistically different to initial concentrations at t = 0 and t = 4 h, as indicated by the asterisk ($p \leq 0.05$).

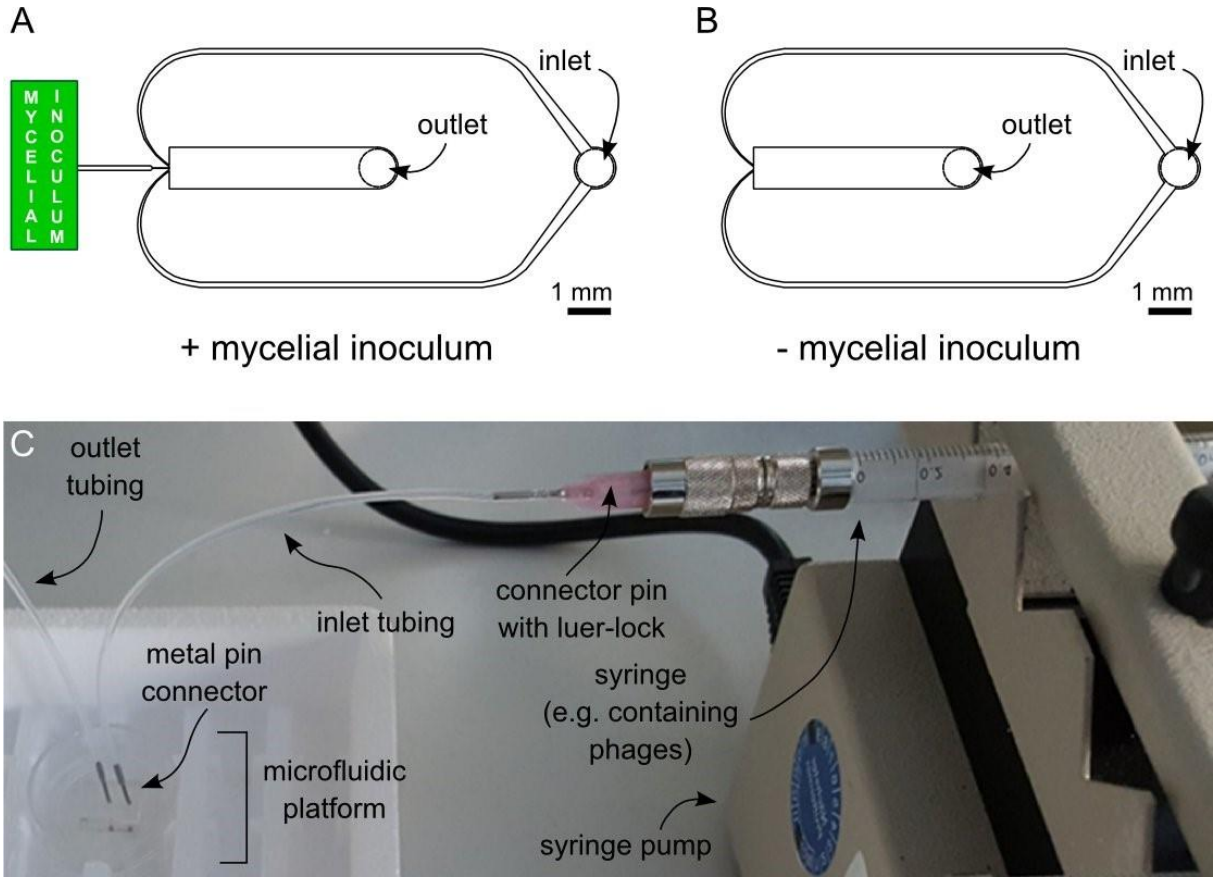

Figure S3. Design and operation of the experimental setup. (A) Two-dimensional representation of the microfluidic platform with a mycelial inoculum that was placed next to the lateral opening of the microfluidic device, allowing hyphae to penetrate and grow into the observation channel via a constriction channel. (B) Two-dimensional representation of the microfluidic platform that enables control measurements to be performed (i.e. in the absence of a mycelium). (C) Photograph illustrating the experimental setup, where a syringe pump was used to drive phage suspensions into the microfluidic channels in the presence and absence of mycelia.

REFERENCES

(1) Stanley, C. E.; Stöckli, M.; Swaay, D. van; Sabotič, J.; Kallio, P. T.; Künzler, M.; deMello, A. J.; Aebi, M. Probing Bacterial–fungal Interactions at the Single Cell Level. *Integr. Biol.* **2014**, *6* (10), 935–945. https://doi.org/10.1039/C4IB00154K.

(2) Stanley, C.; Shrivastava, J.; Brugman, R.; Heinzelmann, E.; Frajs, V.; Bühler, A.; van Swaay, D.; Grossmann, G. Fabrication and Use of the Dual-Flow-RootChip for the Imaging of Arabidopsis Roots in Asymmetric Microenvironments. *BIO-PROTOCOL* **2018**, *8* (18). https://doi.org/10.21769/BioProtoc.3010.

(3) Mavrogiannis, N.; Ibo, M.; Fu, X.; Crivellari, F.; Gagnon, Z. Microfluidics Made Easy: A Robust Low-Cost Constant Pressure Flow Controller for Engineers and Cell Biologists. *Biomicrofluidics* **2016**, *10* (3). https://doi.org/10.1063/1.4950753.

(4) Stone, H. A. Introduction to Fluid Dynamics for Microfluidic Flows. In *CMOS Biotechnology*; Lee, H., Westervelt, R. M., Ham, D., Eds.; Series on Integrated Circuits and Systems; Springer US: Boston, MA, 2007; pp 5–30. https://doi.org/10.1007/978-0-387-68913-5_2.

(5) Chrysikopoulos, C. V.; Syngouna, V. I. Attachment of Bacteriophages MS2 and _X174 onto Kaolinite and Montmorillonite: Extended-DLVO Interactions. *Colloids and Surfaces B: Biointerfaces* **2012**, *92*, 74–83. https://doi.org/10.1016/j.colsurfb.2011.11.028.

(6) Hermansson, M. The DLVO Theory in Microbial Adhesion. *Colloids and Surfaces B: Biointerfaces* **1999**, *14* (1), 105–119.

(7) Van Oss, C. J.; Giese, R. F.; Costanzo, P. M. DLVO and Non-DLVO Interactions in Hectorite. *Clays Clay Miner* **1990**, *38* (2), 151–159.

(8) Attinti, R.; Wei, J.; Kniel, K.; Sims, J. T.; Jin, Y. Virus' (MS2, ΦX174, and Aichi) Attachment on Sand Measured by Atomic Force Microscopy and Their Transport through Sand Columns. *Environmental Science & Technology* **2010**, *44* (7), 2426–2432. https://doi.org/10.1021/es903221p.

(9) Tadros, T. Interfacial Forces in Aqueous Media, Carel J. van Oss, Marcel Dekker Inc., New York, 1994. *J. Chem. Technol. Biotechnol.* **1995**, *64* (3), 311–311. https://doi.org/10.1002/jctb.280640321.

(10) van Oss, C. J.; Docoslis, A.; Wu, W.; Giese, R. F. Influence of Macroscopic and Microscopic Interactions on Kinetic Rate Constants: I. Role of the Extended DLVO Theory in Determining the Kinetic Adsorption Constant of Proteins in Aqueous Media, Using von Smoluchowski's Approach. *Colloids and Surfaces B: Biointerfaces* **1999**, *14* (1–4), 99–104. https://doi.org/10.1016/S0927-7765(99)00028-4.

(11) Van Oss, C. J.; Chaudhury, M. K.; Good, R. J. Interfacial Lifshitz-van Der Waals and Polar Interactions in Macroscopic Systems. *Chemical Reviews* **1988**, *88* (6), 927–941.

(12) Sharma, P. K.; Hanumantha Rao, K. Adhesion of Paenibacillus Polymyxa on Chalcopyrite and Pyrite: Surface Thermodynamics and Extended DLVO Theory. *Colloids and Surfaces B: Biointerfaces* **2003**, *29* (1), 21–38. https://doi.org/10.1016/S0927-7765(02)00180-7.

(13) Boks, N. P.; Norde, W.; van der Mei, H. C.; Busscher, H. J. Forces Involved in Bacterial Adhesion to Hydrophilic and Hydrophobic Surfaces. *Microbiology* **2008**, *154* (10), 3122–3133. https://doi.org/10.1099/mic.0.2008/018622-0.

(14) Van Oss, C. J.; Good, R. J.; Chaudhury, M. K. The Role of van Der Waals Forces and Hydrogen Bonds in "Hydrophobic Interactions" between Biopolymers and Low Energy Surfaces. *Journal of Colloid and Interface Science* **1986**, *111* (2), 378–390. https://doi.org/10.1016/0021-9797(86)90041-X.

(15) Fowkes, F. M. Attractive Forces at Interfaces. *Industrial & Engineering Chemistry* **1964**, *56* (12), 40–52.